STATISTICAL MECHANICS OF COMPLEX NETWORKS AND INTERACTING POPULATIONS

Matti Peltomäki

Department of Applied Physics
Helsinki University of Technology
Espoo, Finland

Dissertation for the degree of Doctor of Science in Technology to be presented with due permission of the Faculty of Information and Natural Sciences for public examination and debate in Auditorium K216 at Helsinki University of Technology (Espoo, Finland) on the 9th of May, 2009, at 12 o'clock.

Dissertations of Department of Applied Physics
Helsinki University of Technology
ISSN 1797-9595 (print)
ISSN 1797-9609 (electronic)

Dissertation 157 (2009):
Matti Peltomäki: Statistical Mechanics of Complex Networks and interacting populations

Opponent:
Prof. Erwin Frey, Universität München, Germany

Pre-examiners:
Prof. Miguel A. Muñoz, Universidad de Granada, Spain
Dr. Claudio Castellano, "Sapienza" Universita di Roma, Italy

ISBN 978-951-22-9852-5 (print)
ISBN 978-951-22-9853-2 (electronic)

Picaset Oy
Helsinki 2009

Abstract

In complex dynamical systems, microscopic processes lead to rich macroscopic behavior. Such are found in a variety of disciplines including complex networks, biological populations, and games. These are studied here using analytical arguments, computer simulations, and analysis of empirical data.

First, bipartite collaboration networks are studied both empirically and numerically. Such graphs consist of two vertex types, actors and ties, and edges are allowed only between vertices with different types. Empirical measurements reveal stretched exponential degree distributions, significant clustering, and assortative mixing together with sublinear preferential attachment. A new growth model for the graphs is introduced and compared to earlier ones and empirics. All considered models predict some properties correctly while failing on several others, emphasizing the need for more developed models.

Next, systems of two interacting populations, hosts and parasitoids, are studied in various environments. The phase diagram is computed both analytically and numerically on a Bethe lattice. The most crucial feature is the lack of a tricritical point: There is no boundary separating phases with both populations alive and both extinct. On scalefree graphs, the parasitoids are shown to behave similarly than the infected nodes in a well-known epidemic model, the susceptible–infected–susceptible model. Consequently, the well-known absense of an epidemic threshold is directly applicable. On square lattices, a similar system with distance-dependent spreading leads to noisy irregular spirals and oscillations with a fluctuating amplitude. The latter is a consequence of a separation of two time scales related to the oscillations. The patterns can also be understood as vortices with topological signs, and measures for the patterning based on these are introduced. Also on an empirical metapopulation landscape serving as the habitat of a butterfly and its parasitoid, spirals form and noise-sustained oscillations are observed.

Finally, pattern formation and extinction probabilities are considered in two-dimensional rock–paper–scissors games, also interpretable as models of three interacting populations. It is known that a four-state variant leads to spirals, and that there is a crossover to extinction when their wave length outgrows the system size. Here, it is shown that with three states spirals do not form, but a length scale leading to a similar crossover still exists. A small asymmetry in the reaction rates is shown not to alter the average wave length of the spirals and thus not to influence the crossover.

Tiivistelmä

Tilastollisen fysiikan systeemeissä mikroskooppiset prosessit johtavat usein rikkaaseen makroskooppiseen käytökseen. Esimerkkejä löytyy muun muassa kompleksisista verkoista, biologian populaatioista ja peleistä. Tässä väitöskirjassa tutkitaan näitä tapauksia analyyttisin argumentein, tietokonesimulaatioin, sekä analysoimalla empiiristä dataa.

Ensiksi tutkitaan kaksiosioisia yhteistyöverkostoja, jotka muodostuvat kahdesta solmutyypistä, toimijoista ja sidoksista, ja linkkejä sallitaan vain erityyppisten solmujen välille. Empiiriset mittaukset osoittavat astelukujakaumat venytetyiksi eksponenttijakaumiksi, suuren klusteroitumisasteen ja positiiviset astelukukorrelaatiot, sekä alilineaarisen etuilevan liittymisen säännön. Uusi verkkojen kasvumalli esitellään, ja sen ennusteita verrataan aikaisempiin malleihin ja kokeellisiin tuloksiin. Kaikki käsitellyt mallit ennustavat osan suureista oikein, mutta epäonnistuvat useissa muissa.

Kahden vuorovaikuttavan populaation, isäntien ja loisten, systeemeitä tutkitaan useissa elinympäristöissä. Bethe-hilalla lasketaan systeemin faasidiagrammi sekä analyyttisesti että numeerisesti. Siinä ei ole trikriittistä pistettä: systeemissä ei ole siirtymää suoraan tilasta, jossa molemmat populaatiot ovat hengissä, tilaan, jossa molemmat ovat sukupuutossa. Mittakaavattomilla verkoilla loiset käyttäytyvat kuten SIS-leviämismallin (susceptible–infected–susceptible) taudinkantajat. Seurauksena tunnettu epidemian nollakynnys yleistyy suoraan. Neliöhilalla havaitaan kohinaisia spiraaleita ja värähtelyjä, joiden amplitudi fluktuoi. Jälkimmäinen seuraa niihin liittyvän kahden aikaskaalan erottumisesta ja kohinasta. Kuviot voidaan ymmärtää topologisesti varautuneina vortekseina, ja useita suureita niiden karakterisointiin esitellään. Samassa systeemissä kokeellisesti mitatussa täpläverkkoperhosen ja erään sen loisen metapopulaatioelinympäristossä on myös kuvionmuodustusta ja melun ylläpitämiä oskillaatioita.

Tässä tutkitaan myös kuvionmuodostusta ja sukupuuttotodennäköisyyksiä kaksiulotteisessa kivi–paperi–sakset-pelissä, joka voidaan tulkita myös kolmen populaation malliksi. Sen nelitilaversion tiedetään johtavan spiraalien muodostumiseen ja sukupuuttoon niiden aallonpituuden kasvaessa systeemin kokoa suuremmaksi. Tässä osoitetaan, että kolmitilaversiossa spiraaleita ei muodostu, mutta systeemissä on silti pituusskaala, joka samoin johtaa sukupuuttoon. Pieni epäsymmetria reaktionopeuksissa ei muuta spiraalien keskimääräistä aallonpituutta eikä sukupuutto-ominaisuuksia.

Preface

This thesis has been prepared at the Department of Applied Physics (formerly Laboratory of Physics) at the Helsinki University of Technology during the years 2004-2008.

I wish to express my gratitude to my instructor Doc. Mikko Alava for all the guidance during my years at the Department of Applied Physics. While a truly original man, he is excellent in the issues an instructor should be good at. I thank Acad. Prof. Risto Nieminen for creating the good working atmosphere in COMP and the facilities supporting research. I am grateful to all my collaborators in this thesis, especially Dr. Martin Rost from whom I have learnt a lot. I also thank Prof. Sergey Dorogovtsev, Acad. Prof. Ilkka Hanski, and Dr. Otso Ovaskainen for useful and inspiring discussions, and the pre-examiners of this thesis, Prof. Miguel A. Muñoz and Dr. Claudio Castellano, for constructive feedback. There are also lots of talented people with whom I have had the pleasure to do science outside the scope of this thesis. Of these, I would like to thank Prof. Olav Tirkkonen, Dr. Erkki Hellén, Hannu Verkasalo, and Markus Ovaska, and the hard-working undergraduate students Juha-Matti Koljonen and Mikael Mohtaschemi. I also wish to acknowledge many people with whom I have had the privilege to discuss at conferences.

All the people at the CSM group are thanked for nice travelling company at various occasions, and for several entertaining evenings playing Koira. Especially Jari Rosti is thanked for all the good servings, Lasse Laurson and Juha Koivisto for all the help with technical issues, and Matti Sarjala for interesting discussions on physics and beyond. I express my sincerest appreciation for all the people at the Department of Applied Physics. Eija Järvinen deserves special thanks for her good sense of humour and helpful attitude.

I would like to thank my mother for all the support.

Finally, my warmest thanks belong to my dear wife Suvi, whose presence, love, and support keeps me going.

Tapiola, March 2009

Matti Peltomäki

Contents

List of Publications

This thesis consists of an overview and the following publications, which are referred to in the text using their Roman numerals.

I M. Peltomäki and M. Alava, "Correlations in bipartite collaboration networks", Journal of Statistical Mechanics: Theory and Experiment, P01010 (2006) (23 pages).

II V. Vuorinen, M. Peltomäki, M. Rost, and M. Alava, "Networks in metapopulation dynamics", European Physical Journal B **38**, 261–268 (2004) (8 pages).

III M. Peltomäki, V. Vuorinen, M. Alava, and M. Rost, "Host–parasite models on graphs", Physical Review E **72**, 046134 (2005) (9 pages).

IV M. Peltomäki, M. Rost, and M. Alava, "Oscillations and patterns in interacting populations of two species", Physical Review E **78**, 050903(R) (2008) (4 pages).

V M. Peltomäki, M. Rost, and M. Alava, "Characterizing spatiotemporal patterns in three-state lattice models", Journal of Statistical Mechanics: Theory and Experiment, P02042 (2009) (31 pages).

VI M. Peltomäki and M. Alava, "Three- and four-state rock–paper–scissors games with diffusion", Physical Review E **78**, 031906 (2008) (7 pages).

The author's contribution

The author has had an active role in all the work reported in this thesis. He has been involved in planning the research. The analytical calculations in Publications **III** and **VI** and partially those in Publications **VI** and **V** have been made by the author. The numerical simulations in Publications **I**, **VI**, **V**, **VI** and the related programming work have been done by him. The numerical simulations in Publications **II** and **III** are due to Ville Vuorinen. The author has collected and analyzed the empirical data in Publication **I** and participated in the analysis in Publication **II**. The author has written Publications **I**, **V**, and **VI**. Publications **III** and **IV** have been written in collaboration with the author having significant responsibility. The author has contributed sections on empirical data analysis to Publication **II**.

1 Introduction

Statistical mechanics deals with macroscopic properties of systems consisting of a large number of elementary constituents, the role of which is typically played by particles [1]. The constituents themselves are usually rather simple, while the beauty of such systems lies in the fact that despite of the simplicity of the parts forming them, large systems tend to have emergent properties: The microscopic bulding blocks of the system interacting with each other act together as a whole in ways that would not even make sense when discussing single particles. Examples of such behavior are phase transitions, pattern formation, and the winner-takes-it-all effect, also known as the Matthew effect [2].

Systems consisting of a large number of similar or almost similar constituents are not restricted to physics only, however. For example, human beings form the constituents of social structures ranging from small circles of closest friends to vast networks of collaborations and mutual dependencies in professional life. Individual animals form together flocks, swarms and so on which in turn combine to populations. Traders in stock markets are the individuals building together the macrosopic outcome of the system – the market rates of the assets. Examples such as these could be listed without any end at sight. A substantial part of them comes from fields outside the traditional domain of physics: Social sciences [3], ecology, and economics [4], to name a few.

In this thesis three families of such systems are studied from the statistical physics point of view. Collaboration networks consisting of scientists and the articles they write together are studied in Section 2 and corresponding results have been published in article **I**. Dynamics of populations are studied in Section 3. In them, not only the populations themselves are the statistical systems under the magnifying lense, but also the space in which they live is quite often built from individual pieces. Results regarding population dynamics have been published in articles **II**, **III**, **IV**, and **V**. A third family of systems is given by games in which individuals change their behavior in search for higher rewards, which in turn depend on the surrounding individuals. This is studied via the rock–paper–scissors game (RPS) in Section 4, and the results have been published in article **VI**.

1.1 Complex networks

Complex networks or graphs have been the topic of intense studies since the 1990s as documented in the review articles and books [5, 6, 7, 8, 9, 10]. A layman's introduction to the topic is given in [11], for example. In general, complex networks are graphs $G = G(V, E)$ consisting of a set of *vertices* or *nodes* V and a set of *edges* or *links* E such that E is a subset of the Cartesian product of V with itself, or $E \subseteq V \times V$. A network can be either undirected or directed. In undirected networks, a link connecting nodes, say, x and y, does not have a direction associated to it, i.e. if $(x, y) \in E$ then $(y, x) \in E$. In directed networks this does not hold. Another generalization is a *weighted graph*, which is a triplet $G = G(V, E, w)$, where V and E are as above and the weight function w assigns each edge a scalar weight. Also weighted graphs can be either directed or undirected. An undirected non-weighted graph is said to be *connected* if every vertex can be reached from every other one by following the links in the graph. A connected graph is said to be *fully connected* if all possible pairs of vertices are linked together, or $E = V \times V$. A network is *bipartite* if there are two kinds of vertices and links are allowed only between pairs of different kinds of nodes.

The networks can be static, but most typically they are formed by a stochastic process, both in theoretical models and in practice. Perhaps the most well-known example of a model network of this kind is the Barabási–Albert network [12], which grows one node at a time as follows. Start from a small fully connected net. At each step, add one node to the network such that it acquires m links to existing nodes. Among them the links are distributed so that the probability that a given existing node gets the link is proportional to its degree. This mechanism is called *preferential attachment*, and it leads to networks with power-law degree distributions $P(k) \sim k^{-\gamma}$ with $\gamma = 3$. Several modifications of the model have also been studied, see e.g. [13, 14, 15, 16, 17], and power-law degree distributions have also been obtained without preferential attachment (for example, [18]). Empirically, similar network growth can be witnessed in networks of scientific articles, for instance, in which the role of the links is played by the citations. There the network grows (roughly) by adding one paper at a time and creating the links from it to the papers it cites.

In this thesis, bipartite growing graphs of scientific collaborations and movies are studied as examples of complex networks. In them the nodes come in two varieties: the social actors (scientists or movie actors) and the social ties

(papers or movies). An actor is connected to a tie if the actor participates in it. In other words, a scientist is connected to an article if he/she appears as a coauthor, and a movie actor is connected to a movie if he/she acted in it. A growth model of such networks is introduced, and it is compared to earlier ones and empirical results below in Section 2.

1.2 Population dynamics

Dynamics of interacting species is a classical problem that has attained interest already in the 1920's [19, 20], and has since been treated in a voluminous body of literature in ecology (e. g. [21, 22]), mathematics, and even statistical physics (e.g. [23, 24, 25, 26, 27]). In such interacting systems, a wide variety of outcomes is possible ranging from oscillatory to stable dynamics [28], and questions regarding under which conditions the dynamics drives populations extinct are among the most important. One recent advance has been the identification of the *extinction debt*, which builds on the idea that the response – i.e. the extinction in the worst case – can be time-delayed with respect to the change in the environment causing it, and that any snapshot observation in time of a given system can be, in fact, in the corresponding transient [29, 30].

Population dynamics can be studied on various kinds of environments. The classical works use a non-spatial setting, also known as mean-field (MF) theory. A straightforward generalization of it is a low-dimensional (typically two) Euclidean space, which is often modelled as a regular square lattice. Also, the complex networks from Section 1.1 can work as the habitat [5, 6, 7, 8, 9]. When it is embedded in two spatial dimensions, correlations – patterns – can build up in a self-organizing way [28]. The type of the patterns spans from spray-like or flame-like in spatial dimensions [31, 32, 33, 34] through ripple-like in space–time [33] to spiral-like [35, 36, 37, 38]. Patterning has also been recovered in statistical physics [39, 40, 41, 42, 43, 44], in chemical surface catalysis reactions [45, 46, 47, 48, 49, 50], in calcium signalling in living cells [51, 52, 53], and in the infamous complex Ginzburg-Landau equation (CGLE) [54]. Also empirical biology is flooded with intriguing examples such as field voles in Northern Britain forming travelling waves [55], mussel beds in the Wadden Sea in the Netherlands with regular spatial patterns [56] together with voles [57] and lemmings [58] in Northern Europe. Recently, similar studies have also been performed in laboratory conditions [59].

The language used to describe and discuss such systems can be individual-based: The elementary dynamical variables of the system can be, say, the number of individuals inhabiting a given lattice site or node of the underlying graph. Such picture appears, needless to say, rather concrete, and the corresponding concepts easily understandable. However, another class of population systems, often in the context of abstract models indistinguishable from the individual-based picture above, is given by *metapopulations* [60, 61]. They are abstract "populations of populations" where a species typically lives on a set of distinct habitat patches, forming rather small local populations. These are not considered through the classical continuous population densities, but via a discrete state space in which the population density ρ_i of node or site i is a Boolean variable: $\rho_i = 1$ if the site is populated, and $\rho_i = 0$ if it is not. Since typically the small local populations are prone to frequent extinctions by chance or by small fluctuations in the environmental variables, but are also easily recolonized by wandering individuals from other patches, the dynamics of metapopulations can be rather rich. In empirical biology, metapopulations appear in a wide variety of different organisms: The spotted owl in Southern California [62], the European nuthatch [63], the land snail *Arianta arbustrorum* in Northern Switzerland [64], water voles in Scotland [65], and the American pika [66] are some examples. From the medical science, an example worth mentioning is the spatial behavior of the HIV in lymphoid tissue [67]. Lately, metapopulations have also been created experimentally in artificial nanofabricated lattices serving as the set of habitat patches for bacteria [68]. However, perhaps the best studied cases are insects, such as the Glanville fritillary butterfly *Melitaea cinxia* on the archipelago of Åland in the Baltic Sea [69, 70, 71].

In this thesis, the emphasis is on a two-population system of the dynamics of a host species and a parasitoid living on its expense in various environments: On Bethe lattices (infinite trees with a constant branching number), on scale-free graphs [12], on regular square lattices, and on an empirically measured metapopulation landscape [70, 71]. This is discussed in more detail in Section 3 below.

1.3 Rock–paper–scissors games

Cyclic dominance of three species is a quite common interaction pattern in Nature. In it three species, say A, B, and C, interact so that A dominates over B, B over C, and C in turn over A. Due to an analogy to a well-known

game, such interaction pattern is commonly referred to as the rock–paper–scissors (RPS) game. Several processes conforming to this picture have been identified in ecology, both spatial [68, 72, 73] and nonspatial [74, 75], and in physics [40, 76, 77, 78, 79] as well as in contexts superficially unrelated to population dynamics such as the public goods game [80].

In general, in noisy systems the RPS game can undergo an extinction process: A given species becomes extinct due to a fluctuation, and it in turn eventually causes the extinction of that of the other species dominating over it. Finally, only the third – essentially randomly selected – species remains alive. Earlier research hints to the direction that small or nonspatial RPS games always lead to extinction [78]. Space stabilizes the system preventing extinctions in practice [76]. On the other hand, the RPS game has been shown to lead to spiral pattern formation in some circumstances [37], and this has an effect how prone the system is to extinction.

In this thesis, the classical RPS game with the three states above and a variant which also explicitly handles empty space are studied together with a version with slightly asymmetric reaction rates. They are compared to each other in terms of the spiral pattern formation and vulnerability to extinction in Section 4.

2 Bipartite collaboration networks

In this Section bipartite collaboration networks consisting of social actors and ties are studied. Especially, a new model for the growth of such networks is introduced and its performance in predicting both basic and advanced network characteristics is evaluated and compared to models previously known from the literature. The results discussed in this Section have been published in article **I**.

2.1 Network topology

There are several ways to characterize networks. The simplest of them is the degree distribution $P(k)$, which is the probability that a randomly selected vertex has the degree k, i.e. it is connected to exactly k other vertices. Typical degree distributions are power laws $P(k) \sim k^{-\gamma}$ and exponential distributions $P(k) \propto e^{-k/k_0}$ where the exponent γ and the characteristic degree k_0 are parameters of the distributions, respectively. However, other forms exist as well, and the classical random networks, also known as Erdös–Rényi graphs [81], have Poissonian degree distributions [5, 6, 7, 8].

The network characteristics describing the degree–degree correlations are derived from the joint degree distribution $P(k, k')$, which is the probability that a randomly selected edge connects nodes with degrees k and k'. Instead of this full two-dimensional probability distribution, the average nearest-neighbour degree (ANND) is often used. It is defined as

$$\bar{k}_{nn}(k) = \langle k \rangle \frac{\sum_{k'} k' P(k, k')}{k P(k)} \,, \tag{1}$$

where $\langle k \rangle$ is the average degree. Due to the summation over k' this quantity is less vulnerable to statistical fluctuations than the joint distribution $P(k, k')$ but naturally less informative. Another aggregated measure for the correlations is the assortativity coefficient [82, 83]

$$r = \langle k \rangle \frac{\sum_k k^2 \bar{k}_{nn}(k) P(k) - \langle k^2 \rangle^2}{\langle k \rangle \langle k^3 \rangle - \langle k^2 \rangle^2} \,. \tag{2}$$

If the network is uncorrelated, the ANND is a constant and the assortativity coefficient r vanishes. Empirical measurement typically yield assortative

mixing (positive r and increasing ANND) for social networks and disassortative mixing for technological networks (negative r and decreasing ANND), although on artificial social networks such as those formed by comic characters the assortativity is not always true [84].

Another important characteristic of networks is the clustering, also known as transitivity. It measures the tendency to find fully connected triangles in the graph. The following definitions are standard in the literature [85]. Let $m_{nn}(x)$ be the number of links between the nearest neighbours of a given vertex x with degree k. Define the local clustering of node x as

$$C_x = \frac{m_{nn}(x)}{k(k-1)/2}\,, \tag{3}$$

where the denominator equals the maximum number of links between the nearest neighbours. Building on this quantity, three widely used definitions for the clustering at the network level are the degree-dependent clustering

$$C(k) = \langle C_x \rangle_k\,, \tag{4}$$

where the average is taken over node with degree k, the average clustering

$$\bar{C} = \sum_k P(k)C(k)\,, \tag{5}$$

and the clustering coefficient

$$c = \frac{\sum_k k(k-1)P(k)C(k)}{\langle k^2 \rangle - \langle k \rangle}\,. \tag{6}$$

In uncorrelated networks, these three definitions coincide.

The preferential attachment (PA) rule can also be considered a network characteristic even though it is related to the network growth process instead of the structure of a static network as such. If the order in which new nodes are added to the network is known, the PA rule can be measured as follows [86]. Let the rule, i.e. the bias to select nodes of degree k, be T_k. The probability that a node added to the network connects to a node with degree k is

$$P_k(t) = \frac{T_k n_k(t-1)}{N(t-1)}\,, \tag{7}$$

where $n_k(t-1)$ is the number of nodes with degree k at time $t-1$, i.e. right before the addition of the new node, and $N(t-1)$ is the total number of nodes in the graph at the same time. Given these, T_k can be measured by building a histogram as a function of the degree k to which each link is added with the weight $N(t-1)/n_k(t-1)$ upon its creation.

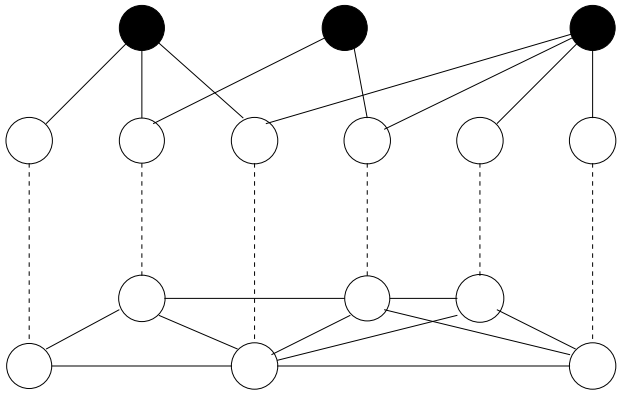

Figure 1: An illustration of the one-mode projection. Above the filled circles denote social ties, the open ones social actors, and the lines the edges between them. Below, each actor is drawn again, now with links between them in the one-mode projection visible, i.e. two actors are connected if they both participate in any given tie.

2.2 Empirical networks

The empirical networks studied in this thesis are bipartite collaboration networks. They consist of two kinds of vertices, called *social actors* and *social ties*, denoting people collaborating with each other in various configurations and the actual collaboration events, respectively. An actor is connected to a tie via an undirected link if the actor took part in the collaboration. The particular networks studied in this thesis are the network of actors and movies from the Internet Movie Database (IMDB) in which an actor is connected to a movie if he/she acted in it, and three author–article networks of scientists and their publications where a scientist is connected to an article if he/she appears as an author of it. The networks correspond to astrophysics (astro-ph), condensed matter physics (cond-mat), and to phenomenology of high-energy physics (hep-ph). The empirical data has been collected from the IMDB web site [87] and from the arXiv.org preprint server [88].

Since the graphs are bipartite, they have two be turned into normal unipartite graphs before the characteristics discussed above are applicable. Note however, that two counterparts of the degree distribution naturally exist in the bipartite presentation, and an analog of the joint degree distribution as well. The graphs are made unipartite by a one-mode projection. In the projection onto actors, two of them are connected by an edge if they have

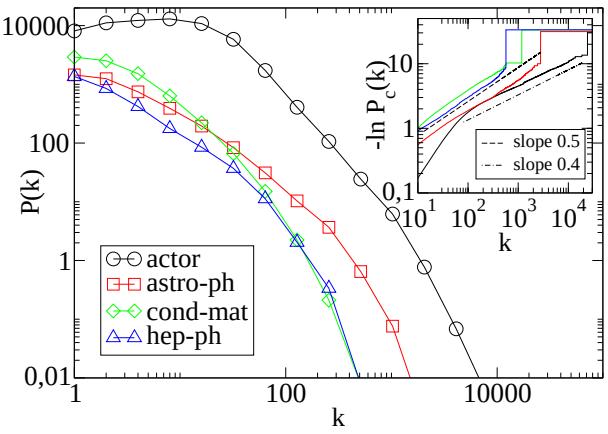

Figure 2: The degree distribution in the one-mode projection onto actors for the different empirical data sets as indicated by the legend. The distributions are clearly not scale-free, but more like of the stretched exponential form (Eq. (8)) with $\alpha \approx 0.5$ in the scientist–article networks as indicated in the inset. The movie–actor network appears to have a power-law region around $k = 100$ but careful examination shows that its tail behavior is also of the stretched exponential form, now with $\alpha \approx 0.4$.

at least one social tie in common. Multiple edges are not allowed. This is illustrated in Fig. 1. The projection onto ties works similarly. Here, the emphasis is mostly on the projection onto actors. In addition to this simple projection method, more elaborated ones have also been discussed recently [89]. The outcome of such methods is a weighted unipartite graph, and they have been shown to be useful also as recommendation algorithms.

The empirically measured degree distributions in the one-mode projection onto actors is shown in Fig. 2. They can be well fitted into the stretched exponential form

$$P(k) \propto k^{-\alpha} \exp(-\frac{\mu}{1-\alpha} k^{1-\alpha}) \,, \tag{8}$$

where μ depends on α and satisfies $1 \leq \mu \leq 2$ [15, 16]. This form has been shown to originate from the growth of unipartite networks with the sublinear PA rule $T_k \propto k^{\alpha'}$ with $\alpha' < 1$ [15, 16]. The actor degree distributions are power laws with a cutoff, and the tie degree distributions are either a power law (the IMDB case) or exponential (the scientist–article case) in the full bipartite graph (see article **I** for details).

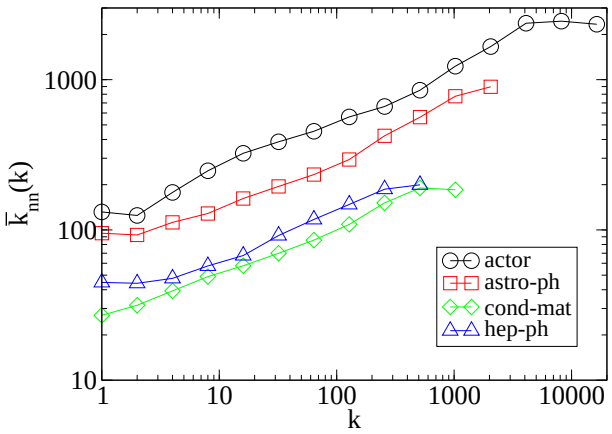

Figure 3: The ANND (Eq. (1)) for the empirical data sets. For each network, a power-law with exponent $\beta \approx 0.3$ can be roughly fitted.

The ANND (Eq. (1)) is plotted in Fig. 3 in the one-mode projection onto actors for all four networks. All of them behave similarly with respect to this quantity: A power-law scaling

$$\bar{k}_{nn}(k) \sim k^{\beta} \tag{9}$$

with $\beta \approx 0.3$ is observed for each. At high degrees k, a cutoff, possibly originating in the finite size of the networks can be seen in each data set. In the one-mode projection onto the ties, the results are similar but with $\beta_{\text{tie}} \approx 0.44$.

The measured effective PA rule is shown in Fig. 4 for the condensed matter physics data set. A power law $T_k \sim k^{\alpha}$ with $\alpha = 0.75$ and a cutoff is recovered. The results for the other data sets are similar with exponents $\alpha \approx 0.65$ for the actor–movie network, $\alpha \approx 0.6$ for the astrophysics network and $\alpha \approx 0.75$ for the high-energy physics network. The figure also shows the measured PA rules for different years to illustrate that the exponent α is indepedent of time. On the other hand, the position of the cutoff increases as a function of time and is therefore most likely a function of the network size. A similar cutoff is also observed when networks are first grown with a PA rule without any cutoff and the PA rule then retroactively measured. Therefore, the the cutoff is merely a finite-size effect. In other words, in networks with finite size, nodes with large enough degrees k are underrepresented which shows up as bias in histograms such as Fig. 4. Later,

a power-law PA rule has also been observed in the growth of the Wikipedia [90].

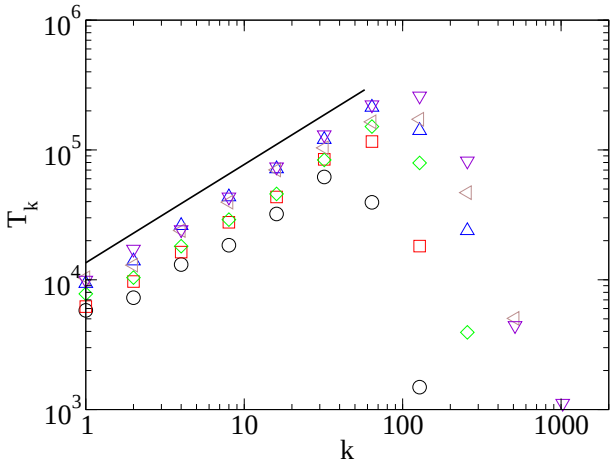

Figure 4: The measured effective PA rule for the condensed matter physics during years 1998 (○), 1999 (□), 2000 (◇), 2001 (△), 2002 (◁) and 2003 (▽), and a corresponding power-law fit (shifted upwards for clarity) with the exponent $\alpha \approx 0.75$.

2.3 Modelling

Growth models for the bipartite collaboration networks have been proposed before. Ramasco *et al.* [83] introduced one in which a bipartite network grows using linear preferential attachment, and augmented it with an aging process of the social actors introducing another factor in the connection probabilities. Guimerá *et al.* [91] proposed a model of team assembly mechanisms in which an artificial triad formation process is added on top of a basic growth model equivalent to the one by Ramasco *et al.* without aging. In it, when a new social tie or collaboration act is created, the first actor to participate is always chosen according to the applied PA rule, but the rest are chosen among those actors that have previously collaborated with the first one with a given probability q and otherwise randomly using the PA rule. This process creates fully connected triangles in the graphs in the spirit of earlier growth models for unipartite graphs [17].

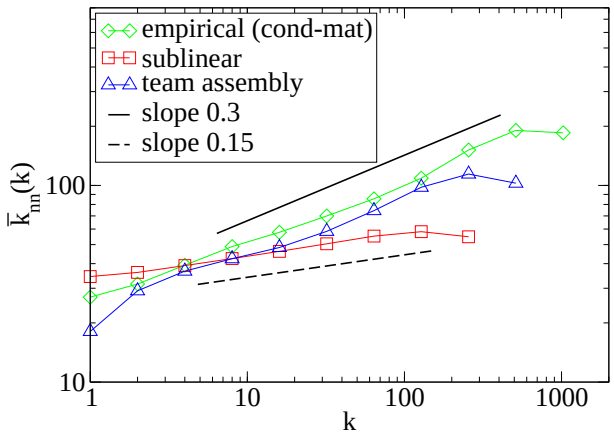

Figure 5: The average nearest-neighbour degree (ANND) in simulations of the introduced model with sublinear preferential attachment ($\alpha = 0.75$) and the team assembly model [91] compared to the empirical measurements. The results from the team assembly model are in reasonable agreement with the empirics, whereas those from the sublinear one roughly scale as a power of k but with a different exponent β. The solid and dashed lines are guides to the eye.

Both of the earlier models outlined above are, however, lacking in the capacity to reproduce the characteristics of the collaboration networks. In particular, the model by Ramasco *et al.* does not reproduce the ANND either without or with aging, nor the PA rule, and the one by Guimerá *et al.* does not reproduce the PA rule since it uses a linear one by definition. To attack these shortcomings, a new growth model for bipartite collaboration nets is introduced in this thesis. It works as follows. At each time step, a new social tie is added to the graph, and the number n of actors connecting to it is chosen at random according to the corresponding empirically measured distribution. The number m of new actors is chosen at random such that each one of the n actors has a given probability p to be a new one, i.e. m is drawn from the binomial distribution. The first of the $n-m$ actors that are not new, is chosen according to the sublinear PA rule $T_k \propto k^\alpha$ from the set of all pre-existing actors. The rest are chosen using the PA rule with probability $1-p_{\mathrm{TF}}$ or at random from the set of earlier collaborators of the previously chosen actor. Defined like this, the most important new element of the model is the incorporation of the sublinear PA rule.

All the considered models reproduce the empirical degree distribution well, together with the degree-dependent clustering (see Eq. (4)). The degree distribution in similar systems has also been later successfully predicted elsewhere (e.g. [92]), and the growing size of both the set of ties and the set of actors has been demonstrated to be a necessary condition for fat-tailed degree distributions [93, 94]. The model introduced here reproduces the ANND qualitatively correctly but with a different exponent $\beta \approx 0.15$. This is shown in Fig. 5. The exponent β is also shown to depend on the PA rule exponent α such that $\alpha = 1.0$ leads to uncorrelated nets with $\beta = 0$ and decreasing α leads to increasing β. The ANND exponent β is in turn shown to be independent of the triad formation probability p_{TF}, which leads to the conclusion that the triad formation process cannot be held responsible for the observed correlations. On the other hand, a similar power-law with $\beta = 0.2$ has been found in a model for unipartite collaboration networks based on geographical proximity [95].

2.4 Outlook

As is clear from above, all growth models introduced so far are inadequate in explaining the structure of the bipartite collaboration networks, and thus there is a clear need for better-performing models. In other words, the attachment rule has to measure the network structure in more detail. One candidate is to use k-connected cliques in analogy to recent observations of their role in network superstructure [96]. They allow for a wide variety of measures for the joint strength of the collaboration of any two given actors. Another way is to exploit the recently introduced social inertia [97] which provides a quantitative time-dependent measure. Also, it is well-known that there are subfields within the different disciplines of science, and these could be taken into account. One way to perform this in an automated data collection procedure is to use the PACS indices as indicators of the subfields in the case of scientist–article networks. Also, a general family of preferential attachment processes is given by rules in which the probability p_i that a new node gets linked to node i is of the form

$$p_i = \frac{x_i^\alpha}{\sum_i x_i^\alpha}\,, \tag{10}$$

where x_i can be any node-spesific time-dependent scalar. The particular case $x_i = k_i$ corresponds to the case of degree-bound preferential attachment

rules studied here. One candidate for x_i for future studies is the betweenness centrality [98] but others can also be envisioned.

3 Two-species dynamics

In this Section, the two-species dynamics on different substrates is studied. First in Section 3.1 the host–parasitoid population models themselves are defined and discussed, and in the following sections their behavior is considered on Bethe lattices, scale-free graphs, square lattices, and on an empirically measured real landscape. The results discussed in this Section have been published in articles **II** (on the empirically measured landscape), **III** (on Bethe lattices and scale-free graphs), **IV** (on square lattices), and **V** (on square lattices and the empirically measured landscape).

3.1 Hosts and parasitoids

The host-parasitoid models studied in this thesis are generalizations of the SIS model [99]. In it, the individuals are in one of two states, either infected (I) or susceptible (S) to an infection. Infected individuals may spread the disease to a susceptible one if both are in contact. On graphs, this means that for spreading they have to live on neighbouring nodes. Infected individuals recover with a given rate irrespective of their surroundings. Altogether, the SIS model is defined by the following reaction rates

$$\begin{aligned} r_{S\to I} &= k_{\mathrm{inf}}\lambda \\ r_{I\to S} &= 1\,, \end{aligned} \tag{11}$$

where k_{inf} is the number of infected neighbours of the node.

In this thesis, a generalization of the SIS model to systems with two populations, hosts and parasitoids, is studied. In these, the individuals can be in one of three different states: Empty (E), populated by the host (H), or populated by both the host and the parasitoid (P). Between these states, there are six possible transitions with the following rates

$$\begin{aligned} r_{E\to H} &= k_{\mathrm{h}}\lambda \\ r_{H\to P} &= k_{\mathrm{p}}\alpha\mu \\ r_{H\to E} &= 1\,, \\ r_{E\to P} &= 0\,, \\ r_{P\to H} &= \epsilon\,, \\ r_{P\to E} &= \alpha\,, \end{aligned} \tag{12}$$

where k_{h} and k_{p} are the numbers of neighbours inhabited by the hosts and the parasitoids, respectively. As above, the decay rate of the hosts sets the

time scale. Only cases in which the parasitoids do not decay on their own, i.e. $\epsilon \approx 0$ are considered.

As an alternative to the formulation above which works on any graph, one can consider cases where the nodes are embedded in such a space that allows for a definition of a (Euclidean) distance between the nodes. In these cases, one does not have to restrict the spreading to nearest neighbours only, but it can be generalized to be distance-dependent. In this setting, at each node the transition probabilities from a state to another depend on the surrounding populations through the connectivity

$$I_\alpha(\mathbf{x}, t) = \sum_{\mathbf{x}' \in V} k_\alpha(|\mathbf{x} - \mathbf{x}'|)\chi_\alpha(\mathbf{x}', t)\,, \tag{13}$$

of node $\mathbf{x}$ with respect to species α (H or P). Here, V is the set of all nodes, and $\chi_\alpha(\mathbf{x})$ is the characteristic function, i.e. $\chi_\alpha(\mathbf{x}) = 1$ if the state of node $\mathbf{x}$ is α and $\chi_\alpha(\mathbf{x}) = 0$ otherwise. The kernel k_α decays exponentially with the species-dependent scale parameter w_α and is normalized by $\sum_{\mathbf{x}' \in V} k_\alpha(|\mathbf{x}|) = 1$. Motivations for this particular form for the connectivity come from biology [61]: They naturally incorporate the distance-dependence of migration-induced recolonization in metapopulations, and the parameters within have been succesfully estimated from empirical studies (e.g. [100]).

In the version of the model with distance-dependent spreading, the probabilities from the transitions per time step are as follows. The transition $E \to H$ takes place with probability $\min(1, \lambda_h I_h)$, $H \to P$ with probability $\min(1, \lambda_p I_p)$, and the parasitoids die (transition $P \to E$) with probability δ irrespective of the surroundings. Note that, differently from above, the parasitized hosts do not reproduce. This difference again is motivated by biology: The reproductive capability of hosts being under the influence of parasitoids can be severely decreased. Note also that the symbols for the spreading rate parameters λ_h and λ_p have been changed to emphasize the conceptual difference between the two models.

So far, the language used in the definition of the models has been individual-based: The nodes in the graph are considered either empty or hosting a single individual of a species. However, all the variants of the present models can be also understood as ones describing the behavior of the metapopulations discussed in Section 1.2.

3.2 Bethe lattices

The simplest substrate on which the host–parasitoid models are studied in this thesis, is the Bethe lattice, also known as a Cayley tree. It is an infinite tree with a constant branching number z. Since the structure is a tree, any analytical treatment is crucially simplified by the fact that the subtrees emanating from any given node are by definition independent in terms of the population dynamics. However, finite-size approximations are needed for numerical simulations. If the tree is merely truncated to a given number of nodes, an extensive number of leaf nodes with only one neighbour remains. The fraction of these does not vanish even at the limit of infinite number of nodes, and the leaf nodes introduce a serious bias in the simulations.

This difficulty can however be overcome by constructing sparse homogeneous graphs that closely approximate the Bethe lattice without any leaf nodes. The prodedure is due to Dhar [101] and in it a regular one-dimensional ring is first created and the missing $z-2$ links per node are put in place by generating $z-2$ random orderings of the nodes and in each ordering by connecting the first node to the second one, the third to the fourth, and so on. While this method is not necessarily an optimal way of closing the Bethe lattice, it has some serious advantages: Short loops are absent in the thermodynamic limit, and all nodes have exactly the same coordination number.

On the Bethe lattice, the SIS model has a known mean-field (MF) solution [102]. In this thesis, the solution is extended both to the HP model and to more refined approximation schemes. In short, the phase diagram is calculated analytically in three different approximative ways and numerically from direct simulations of the model. The first way is the MF approximation, also known as the singlet approximation. It is defined by the rate equations

$$\partial_t \rho_h = -\rho_h + \lambda(1-\rho_h-\rho_p)\Theta - \alpha\mu\rho_h\Phi\,, \tag{14}$$

$$\partial_t \rho_p = -\alpha\rho_p + \alpha\mu\rho_h\Theta \tag{15}$$

for the host and parasitoid densities ρ_h and ρ_p. Here, $\Phi = 1-(1-\rho_p)^z$ and $\Theta = 1-(1-\rho_h)^z\cdot$ In the absence of the parasitoids the state $\rho_h = 0$ is stable if and only if $\lambda \leq 1/z$ and therefore the boundary between an empty phase and an active phase with at least the hosts alive is given by $\lambda = 1/z$. Similarly, the pure host phase is stable if parasitoids cannot invade. This

condition is given by the equation

$$\mu \leq \frac{1}{z\rho_h}\,, \tag{16}$$

where ρ_h is the host density when the parasitoids are absent.

The remaining two analytical calculations are variants of the pair – or doublet – approximation. Such have been previously used for a spatially uniform insect host–parasitoid model [103, 104], for the contact process in a one-dimensional chain [105], for other related systems [106, 107], and in general over a wide class of models [108]. The pair approximation starts from the following rate equations

$$\partial_t \rho_h = (-1 - z\alpha\mu\rho_{p|h} + z\lambda\rho_{e|h})\rho_h\,, \tag{17}$$

$$\partial_t \rho_p = (-\alpha + z\alpha\mu\rho_{h|p})\rho_p\,, \tag{18}$$

$$\partial_t P_{hh} = -[2 + 2(z-1)\alpha\mu\rho_{p|h}]P_{hh} + \lambda[1 + (z-1)\rho_{h|e}]P_{he}\,, \tag{19}$$

$$\begin{aligned}\partial_t P_{hp} = &-\{1 + \alpha + \alpha\mu[1 + (z-1)\rho_{p|h}]\}P_{hp} \\ &+(z-1)\lambda\rho_{h|e}P_{pe} + 2(z-1)\alpha\mu\rho_{p|h}P_{hh}\,,\end{aligned} \tag{20}$$

$$\partial_t P_{pp} = -2\alpha P_{pp} + \alpha\mu[1 + (z-1)\rho_{p|h}]P_{hp}\,, \tag{21}$$

$$\begin{aligned}\partial_t P_{he} = &-\{1 + (z-1)\alpha\mu\rho_{p|h} + \lambda[1 + (z-1)\rho_{h|e}]\}P_{he} \\ &+2(z-1)\lambda\rho_{h|e}P_{ee} + 2P_{hh} + \alpha P_{hp}\,,\end{aligned} \tag{22}$$

$$\partial_t P_{pe} = -[\alpha + (z-1)\lambda\rho_{h|e}]P_{pe} + (z-1)\alpha\mu\rho_{p|h}P_{he} + P_{hp} + 2\alpha P_{pp}\,, \tag{23}$$

$$\partial_t P_{ee} = -2(z-1)\lambda\rho_{h|e}P_{ee} + P_{he} + \alpha P_{pe} \tag{24}$$

for the joint probabilities $P_{\sigma\sigma'}$ that a randomly selected edge between two nodes has its endpoints in states σ and σ'. They can be expressed in terms of the conditional probabilities as

$$P_{\sigma\sigma'} = \rho_\sigma \rho_{\sigma'|\sigma}(2 - \delta_{\sigma,\sigma'})\,, \tag{25}$$

where $\delta_{\sigma,\sigma'}$ is the Kronecker symbol.

With parasitoids absent, the stability of the absorbing solution $\rho_h = 0$ can be easily studied, and it is recovered that it is unstable if $\lambda \geq 1/(z-1)$. This should be compared with the result $\lambda \geq 1/z$ for the mean-field approximation arrived at above.

Two approximative solutions for the doublet approximation are presented here. The first one starts by defining two auxiliary quantities, $A = \rho_{h|p}$ and $B = \rho_{h|p} + \rho_{p|p}$. The rate equation for A reads

$$\frac{\partial A}{\partial t} = \frac{\partial}{\partial t}\frac{P_{hp}}{2\rho_p} = \frac{1}{2\rho_p}\left(\frac{\partial P_{hp}}{\partial t} - P_{hp}M_p\right) , \tag{26}$$

where $M_p = -\alpha + \alpha\mu z$. Plugging Eq. (20) into Eq. (26), using Eq. (25) and looking at the limit of vanishing parasites one arrives at

$$2z(z-1)(1-B)\lambda^2 +$$

$$\{2z^2\alpha\mu A(1-A) + 2z[B-1-A(1+2\alpha\mu)]\}\lambda - 2(z-1)A\alpha\mu = 0\,. \tag{27}$$

Similarly, one can write the rate equation for B,

$$\frac{\partial B}{\partial t} = -\frac{\partial \rho_{e|p}}{\partial t} = \frac{1}{2\rho_p}\left(P_{ep}M_p - \frac{\partial P_{ep}}{\partial t}\right) . \tag{28}$$

Using Eqs. (23) and (25), one gets

$$2z(z-1)(1-B)\lambda^2 + 2z^2\alpha\mu A(1-B)\lambda$$

$$+2z[(B-A)(1-\alpha)-1]\lambda - 2(z-1)A\alpha\mu = 0 \tag{29}$$

given that $\lambda \neq 0$.

Now solve for A from the steady-state version of Eq. (18), substitute it in Eqs. (27) and (29), and eliminate B from the resulting two equations to arrive at the expression for the phase boundary as

$$\mu = \frac{z(z-1)\lambda^2 + z\alpha\lambda}{z(z-1)^2\lambda^2 + z[(z-1)(\alpha-1)-\alpha]\lambda + \alpha(1-z)}\,. \tag{30}$$

The second approximative solution to the pair approximation rate equations starts by linearizing them at the fixed point with hosts alive and parasitoids extinct. Doing this, one arrives at a linearization matrix of the form

$$M = \begin{pmatrix} M_h & M_{hp} \\ 0 & M_p \end{pmatrix} , \tag{31}$$

where M_h governs the stability of the solution with hosts alive, M_{hp} describes the effect of a small parasitoid population on the hosts, and M_p

the growth of the parasitoids at low densities. The lower left block is zero since the state without parasitoids is an absorbing state in terms of the dynamics. The stability of the solution with parasitoids alive can be deduced from the largest eigenvalue of the 4×4 submatrix M_p: If it is larger than zero, the solution is stable. The stability boundary has been obtained by numerically solving for the eigenvalues and searching for the zero using an iterative forking procedure.

The phase diagram of the host–parasitoid model obtained from all the three analytical solutions and from direct numerical simulations can be seen in Fig. 6. In each case, the two-dimensional parameter space spanned by μ and λ is divided into three phases: An empty one with both populations extinct, a parasitoid-absorbing phase with a living host population but parasitoids extinct, and a coexistence phase with both populations alive. All phase boundaries in the Figure are in qualitative agreement with each other.

The most notable property of the phase diagram is the lack of a tricritical point. In other words, there is no boundary separating the empty and the coexistence phases. This can be seen direcly from Eq. (16) since the critical value of the parasitoid spreading rate approaches infinity as the host population size approaches zero, and also from Eq. (30) by a direct limit value calculation at the limit $\mu \to \infty$.

3.3 Scalefree graphs

The SIS model has been formulated on standard scalefree Barabási–Albert graphs [12] in [102]. In the thesis, the formulation is extended to the host–parasitoid model and the corresponding rate equations in the mean-field approximation for the degree-dependent population densities ρ_h^k and ρ_p^k are

$$\partial_t \rho_h^k(t) = -\rho_h^k(t) + \lambda k[1 - \rho_h^k(t) - \rho_p^k(t)]\Theta_k(\mu, \lambda) - \mu\alpha k \rho_h^k(t)\Phi_k(\lambda, \mu)\,, \quad (32)$$

$$\partial_t \rho_p^k(t) = -\alpha \rho_p^k(t) + \mu\alpha k \rho_h^k(t)\Phi_k(\lambda, \mu)\,, \quad (33)$$

where $\Theta_k(\lambda, \mu)$ and $\Phi_k(\lambda, \mu)$ are the probabilities that a given link emanating from a node with degree k points to an infected or a parasitized host, respectively. It is known that in the SIS model governed by these equations without any parasitoids, there is no nonzero epidemic threshold if the degree distribution is fat-tailed [102]. This holds even on networks with arbitrary degree–degree correlations [109].

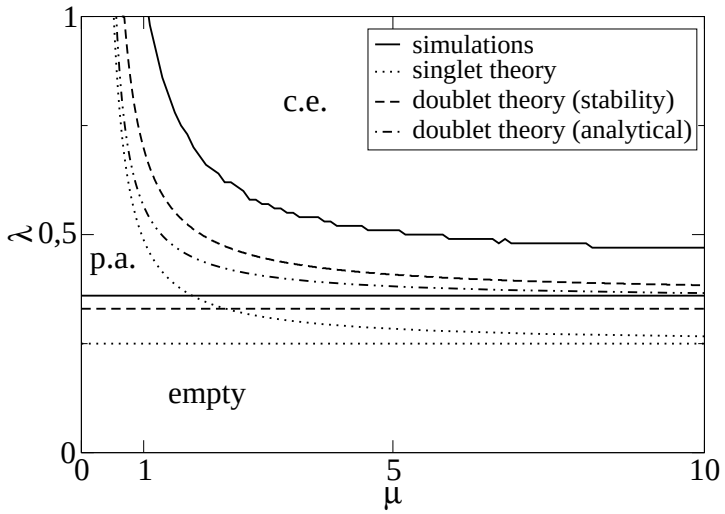

Figure 6: Phase diagram for the host–parasitoid model on the Bethe lattice with the braching number $z = 4$ in the (λ, μ)-plane with $\alpha = 1.2$ and $N = 40000$ nodes calculated from the mean-field approximation, from the pair approximation in both ways, and from direct numerical simulations. In all cases the parameter space is divided into an empty phase, a parasitoid-absorbing (p.a.) phase with only hosts alive, and a coexistence (c.e.) phase with both populations alive. The horizontal lines are the boundaries between the empty and the parasitoid-absorbing phases, and the upper lines are the boundaries betwween the parasitoid-absorbing and coexistence phases.

However, in a model closely resembling the SIS model, the contact process, there is a finite threshold [110, 111, 112, 113]. The SIS model can be turned into the contact process by dividing the outward spreading rate from a node with degree k by k. If the degree were a constant, this change would be merely a scaling of the spreading rate parameter, but in networks with fat-tailed degree distributions the difference can be huge, and deviations from the corresponding MF theory are observed [110]. One can also construct a "double contact process" as a counterpart of the HP model, with the the same dynamics by dividing the outward spreading rate by the degree k for both the hosts and the parasitoids. It is expected, especially in the light of the results sumarized below, that in that case the behavior of the parasitoids conforms to the same picture, both when the existence of the epidemic threshold and the deviations from the MF are concerned.

Let us first consider the case where the host population is substantial enough so that the feedback on the parasitoids can be neglected. The calculation outlined below is a straightforward generalization of one presented in [109] for the SIS model on correlated networks. It starts from Eq. (33) cast in the form it assumes on correlated graphs

$$\frac{\partial}{\partial t}\rho_p^k = -\alpha\rho_p^k + \alpha\mu\rho_h^k\phi_k\,, \tag{34}$$

where $\phi_k = \sum_{k'} k\Delta_{kk'}\rho_p^{k'}$ and $\Delta_{kk'} = P(k'|k)$ is the matrix of the conditional probalities that starting from a node of degree k and following a random edge one arrives at a node of degree k'. Considering at first a system with a finite cutoff degree k_c so that the parasitoid densities form a finite-dimensional vector $\rho = (\rho_p^1 \cdots \rho_p^{k_c})^T$ and Eq. (34) can be cast as a linear time-evolution equation

$$\frac{\partial}{\partial t}\rho = (-\alpha I + \alpha\mu\rho_h^k k\Delta_{kk'})\rho = (-\alpha I + \alpha\mu C_{kk'})\rho\,, \tag{35}$$

where $C_{kk'} = \rho_h^k k\Delta_{kk'}$.

From here, the stability of the parasitoid population can be deduced from the properties of the matrix $C_{kk'}$ or, more precisely, eigenvalues thereof. It has been shown in this thesis that its largest eigenvalue diverges at the thermodynamic limit $k_c \to \infty$. Physically, the origin of this property can be understood as follows. The average nearest-neighbour degree diverges at the thermodynamic limit, which is equivalent to the divergence of the second moment of the degree distribution, and that the same quantity averaged over only nodes populated by a host diverges as well, since even though the degree-dependent host density ρ_h^k is an increasing function of the degree k it has to saturate to a constant asymptotic value for large degrees k. Once this has happened, the dilution of the network from considering only the nodes inhabited by the host is uniform at the MF level, and the resulting effective graph for the parasitoid spreading can be regarded as a standard scalefree network.

Also the rate equations from the pair approximation can be formulated on scale-free graphs. Here, the notation is as follows. Let $P_{\sigma\sigma'}^{kk'}$ be the probability that a randomly chosen edge that connects nodes with connectivities k and k' is such that the state of the node with connectivity k (k') is σ (σ'). Similarly, let $Q_{\sigma\sigma'}^{kk'}$ be the conditional probability that a randomly chosen edge that connects nodes with degree k and k' is such that the state of the

node with connectivity k' is σ' conditioned that the state of the node with connectivity k is σ. Using this notation, rate equations for the SIS model can be written as follows

$$\partial_t \rho_h^k = -\rho_h^k + \lambda \sum_{k'} k \Delta_{kk'} P_{eh}^{kk'} \,, \tag{36}$$

$$\partial_t P_{hh}^{kk'} = -2P_{hh}^{kk'} + \lambda P_{he}^{kk'} + \lambda \sum_{k''} \Delta_{k'k''} P_{he}^{k''k'} (k'-1) Q_{eh}^{k'k} \,. \tag{37}$$

To draw qualitative conclusions for the HP model only the rate equation for the singlet parasitoid density

$$\partial_t \rho_p^k = -\alpha \rho_p^k + \mu\alpha \sum_{k'} k \Delta_{kk'} P_{hp}^{kk'} \tag{38}$$

is needed. Namely, consider the steady-state and multiply Eq. (38) by $P(k)$ and sum over k to get

$$\rho_p = \mu P_{hp} \,. \tag{39}$$

In other words, at the steady state the size of the parasitoid population is directly proportional to the number of links connecting nodes with states h and p. This in turn tells that the dynamics of the parasitoids at the steady-state has to be similar to that of the number of infected individuals in the SIS model, since in it the number of edges that can spread the infection is proportional to the number of infected individuals.

To summarize, both the mean-field approximation and the doublet approach lead to the conlusion that the behavior of the parasitoids in the HP model is similar to the behavior of the hosts, both regarding the dynamics and the absorbing-state transition. These results have also been confirmed numerically in Monte Carlo simulations due to Ville Vuorinen in article **III**.

3.4 Square lattices

In this thesis, the version of the HP model with distance-dependent spreading according to the connectivity in Eq. (13) and the transition rates below it has been studied on regular square lattices with periodic boundary conditions. The first and foremost observation of such studies is that, in a certain region of the parameter space, spatial correlations – patterns – build up. Examples of these can be found in Fig. 7. As discussed in Section 1.2, such pattern formation is ubiquitous.

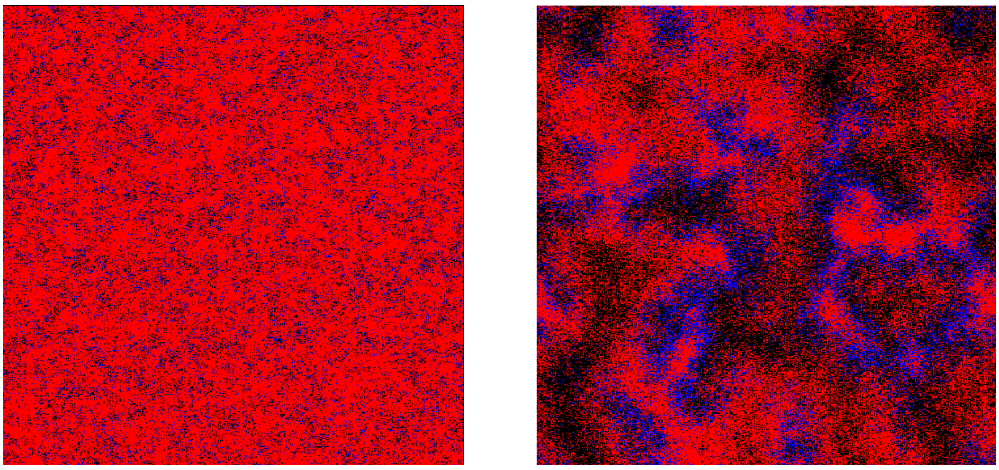

Figure 7: Two examples of the HP model with connectivity-driven spreading with both populations alive. Left: disordered homogeneous structure for parameters $w_h = 3.0$, $w_p = 1.5$, $\lambda_h = 0.63$, $\lambda_p = 1.3$ and $\delta = 0.9$. Right: a patterned state; parameters are as in the non-patterned one except for $\lambda_p = 2.5$. Empty sites are black, red stands for hosts, and blue for parasitoids.

The second immediate observation is that the global dynamics as seen through the average population densities bears highly different signatures depending on the presence or absence of the patterns: Without them the densities fluctuate around the respective averages, whereas with patterns oscillations with erratically fluctuating amplitudes are recovered. See Fig. 8 for the corresponding population densities as a function of time.

The pattern formation and the global dynamics form the two focal points of the analysis presented here. These are not separate issues, however, but mutually connected. They are linked by the fact that the spatial correlations modify the global dynamics with respect to the dynamics of a fully mixed system, and the mechanism of this modification is pinpointed to lie in the response of the interaction rates to instantaneous population densities below.

3.4.1 Pattern formation

To characterize the patterns, a method to coarse-grain them into areas dominated by either species or empty space is introduced. It starts by

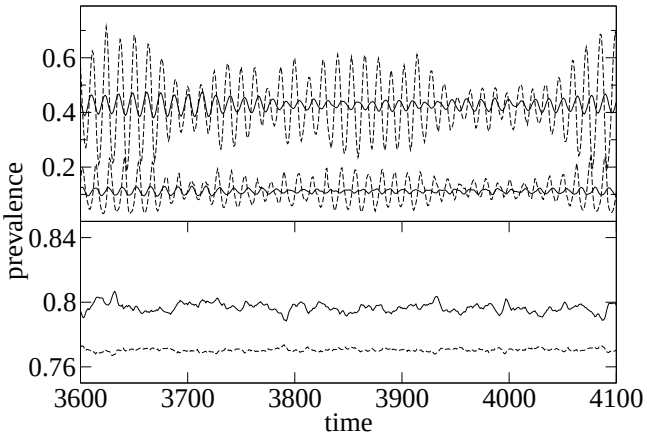

Figure 8: Upper panel: the population densities in the patterned state of the HP model with distance-dependent spreading for a lattice of size $L = 512$ (solid lines), and a sublattice of size $L = 64$ (dashed lines) of a similar one. The upper curves correspond to hosts and the lower ones to parasitoids. The parameters are as in Fig. 7. Lower panel: the population densities in the homogeneous state for the hosts (solid line) and parasitoids (dashed line) for $L = 512$. The parasitoid curve has been shifted upwards for clarity. The parameters are as in the upper panel except for $\lambda_p = 1.3$.

considering spatially convoluted continous fields of population densities

$$\rho_{h|p,w}(\mathbf{x}, t) \equiv \sum_{x'} k_w(|\mathbf{x} - \mathbf{x}'|)\chi_{h|p}(\mathbf{x}', t)\,, \tag{40}$$

where the smoothing kernel $k_w(\mathbf{x})$ is a two-dimensional Gaussian such that $\sum_{\mathbf{x}} k_w(\mathbf{x}) = 1$, $\sum_{\mathbf{x}} \mathbf{x} k_w(\mathbf{x}) = 0$, and $\sum_{\mathbf{x}} \mathbf{x}^2 k_w(\mathbf{x}) = w^2$. The width w of the Gaussian is called here the smoothing width. At each lattice site $\mathbf{x}$, the smoothed densities $\rho_{h|p,w}(\mathbf{x}, t)$ oscillate around the temporally and spatially averaged densities $\bar{h}$ and $\bar{p}$. These are used to divide the two-dimensional space of the densities intro three sectors corresponding to empty space, hosts, and parasitoids as follows. The boundary between the regions corresponding to hosts and parasitoids is the half-line starting from $(\bar{h}, \bar{p})$ going toward higher densities whose continuation to the opposite direction passes through the origin. The two other boundaries form 120-degree angles with the first one and with each other. A lattice site $\mathbf{x}$ at time t then belongs to the domain according to the region of the phase space that contains the corresponding local smoothed population densities $(\rho_{h,w}(\mathbf{x}, t), \rho_{p,w}(\mathbf{x}, t))$. Here,

the domains so formed are called *prevalence domains*. An illustration of the division of the phase space into sectors and an example of the prevalence domains can be found in Fig. 9.

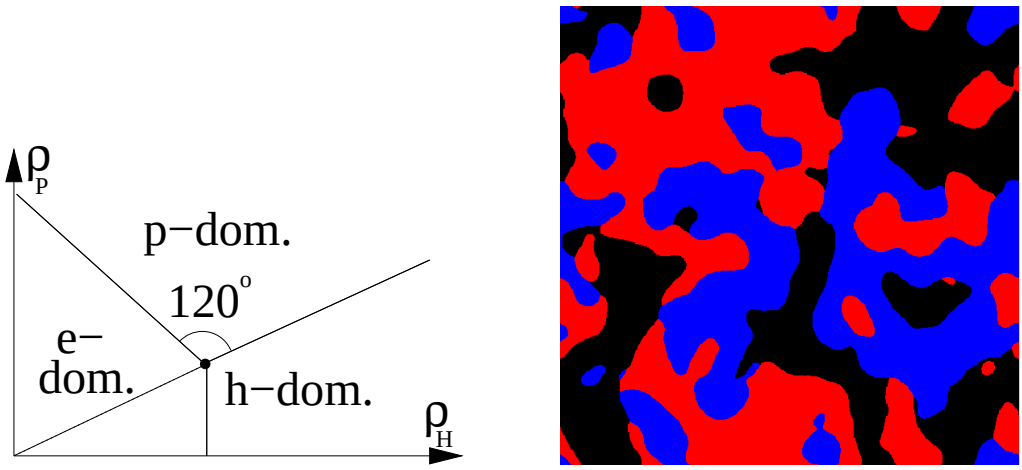

Figure 9: (a) The division of the phase space into three sectors associated with the three states, e, h and p. For given average densities $\bar{h}$ and $\bar{p}$, the first quadrant of the (ρ_h, ρ_p)-plane is divided into three regions by three lines. That separating h- and p-dominated regions starts from the average $(\bar{h}, \bar{p})$ (the black dot), goes towards increasing ρ_h and ρ_p, and is such that its continuation (the dotted line) passes through the origin. The other two lines form 120-degree angles with the first one and each other. (b) The computed dominance regions of the configuration shown in Fig. 7.

The prevalence domains themselves serve as an intermediate stage in defining aggregated quantities describing the geometry and dynamics of the patterns. First, the corner points of three different types of domains form *vortices* associated with a sign, since the three domains can be encountered in two different orders when traversing a small cycle around the vortex, say, counter-clockwise. The boundary lines form *domain walls*. See Fig. 10 for an illustration. A method to track the motion of both the vortices and the domain walls in time has been developed in this thesis (see article **V** for details of the procedure), and it is subsequently used to analyze the patterns.

Similar structures with three kinds of domains rotating around their corner points without any coarse-graining have been identified earlier in statistical

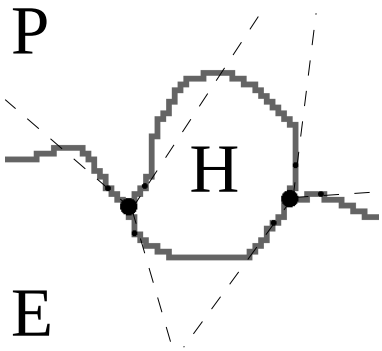

Figure 10: An illustration of the vortices, the domain walls, and the tangents of them describing the geometry of the walls near the vortices. The background is a magnified portion of Fig. 9b with all three domains colored white and marked with capital letters, and the boundaries marked gray. The locations of the vortices are shown with thick black circles. The smaller black circles show lattice sites on the wall that are at the distance of $w_t = 5$ lattice units from the vortices, and the dashed lines drawn via the vortices and these points are the domain wall tangents.

physics in the context of the three-state voter model [40], the extended three-state voter model and the three-state Potts model [77], and combinations thereof [41, 44]. Also a four-state model with game-theoretical inspirations [114] shows similar vortices. In three dimensions, the vortices generalize to strings [31].

In general, all quantities defined via the vortices and the domain walls are able to see the division of the parameter space into patterned and non-patterned domains. Here, two examples are considered. More can be found in Publication **V**. The first example is the distribution of the instantaneous velocities of the vortices, i.e. the distances moved by the vortices in unit time. The second one is given by the distribution of the lifetimes of the vortices. Both are plotted in Fig. 11 for the patterned and non-patterned cases. The difference between them is rather huge is both quantities, and even enormous in the vortex lifetime.

A yet further example is given by the average domain wall length. Since there are domains in the non-patterned case that originate in random fluctuations, a wall length of zero is not the proper null hypothesis. Instead, the average wall length in random configurations is considered. There, systems

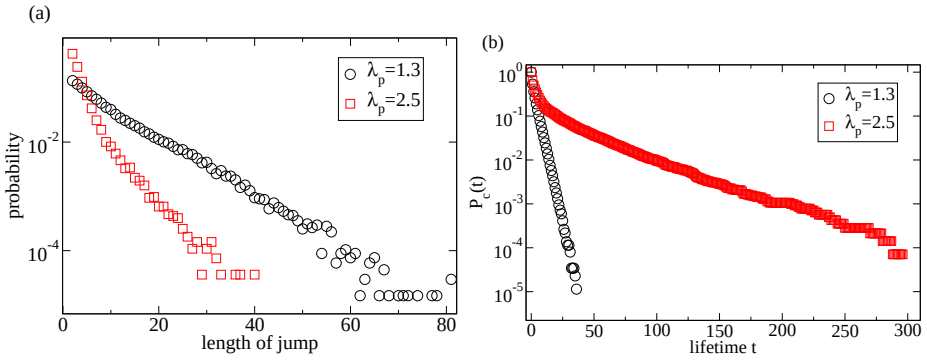

Figure 11: (a) Distribution of the jump length of the vortices, i.e. the distance traveled by a vortex in unit time, in both the non-patterned ($\lambda_p = 1.3$) and the patterned ($\lambda_p = 2.5$) case. Other parameters are as in Fig. 7. The average jump lengths are approximately 3.6 and 9.2 lattice units for $\lambda_p = 2.5$ and $\lambda_p = 1.3$, respectively. (b) The cumulative distribution function of the vortex lifetime in the same two cases. The average lifetimes are approximately 2.9 and 8.7 discrete-time units for $\lambda_p = 1.3$ and $\lambda_p = 2.5$, respectively.

in which the states of individual lattice sites are assigned uniformly at random using the ensemble-averaged population densities as the probabilities are created and the average domain wall length is computed from them. After this, the ratio of the actual average wall length in real simulations to its counterpart in the random configurations becomes a reasonable metric for the patterning. Values near one signal spatially homogeneous systems whereas those clearly larger than one are signs of spatial correlations or patterning. Thege wall length ratio is plotted in Fig. 12 as a function of the spreading rate parameters and also clearly dinstinguishes between the two cases.

3.4.2 Global dynamics

As shown above in Fig. 8, the global dynamics of the system in the patterned case comprises of oscillations with an erratically fluctuating amplitude. These oscillations do not conform to the classical limit cycle picture. This can be demonstrated and explained as follows. First, the Poincaré maps in Fig. 13 illustrate the dynamics of the system, as measured from

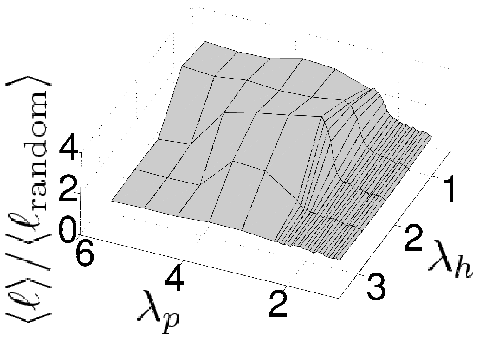

Figure 12: The ratio of the measured average domain wall length to its counterpart in random configurations as a function of the parasitoid and host spreading rate parameters λ_p and λ_h. The ratio is approximately one in the uniformly distributed case and increases to approximately three in the patterned case. In all cases, the distribution of the domain wall lengths decays exponentially (not shown). Other parameters are as in Fig. 7.

simulations. In them, the population densities h_{t+1} and p_{t+1} at time $t+1$ are plotted as a function of the same densities h_t and p_t at the previous time step, i.e. at time t. One sees immediately that the densities are unique functions (up to noise) of their previously assumed values and that for systems large enough – such as the one shown in the Figure – this dependence is even linear.

Based on the numerical observations, the dynamics is satisfactorily described in terms of two dynamical variables, the global densities, and it is linear in these variables:

$$\begin{aligned} h_{t+1} &= a_{h,h} h_t + a_{h,p} p_t + c_h \\ p_{t+1} &= a_{p,h} h_t + a_{p,p} p_t + c_p \quad . \end{aligned} \tag{41}$$

Such two-dimensional linear mappings are completely described in terms of the eigenvalues of the matrix involved. In oscillatory cases, they form a complex-conjugated pair $\rho e^{\pm i\phi}$, where $\rho < 1$ always in the two-dimensional systems studied here. In other words, the fixed point of the system is stable. The pair is in turn associated with two time scales: The time of a period and the inverse decay rate of the amplitude. The crucial quantity for the dynamics turns out to be the ratio of these two time scales

$$\nu = \phi / |\ln \rho| \, . \tag{42}$$

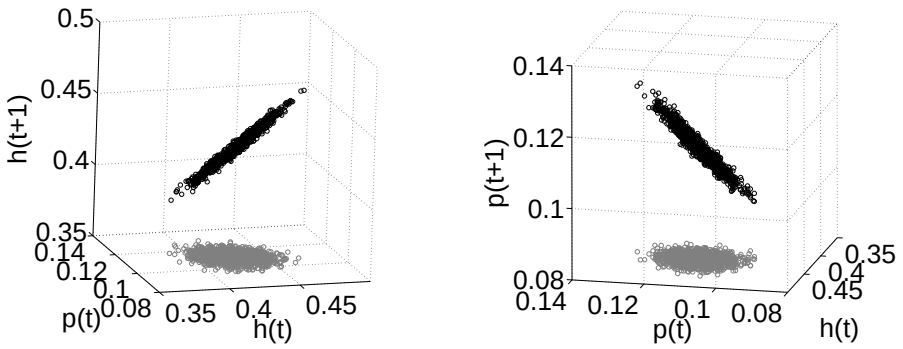

Figure 13: Left: h_{t+1} over h_t and p_t (black) in a perspective showing the planar arrangement of points and its projection onto the (h_t, p_t)-plane (gray). Right: the same for p_{t+1}. Parameters are as in Fig. 7.

Large values of ν indicate that the dynamics is oscillatory whereas for values $\nu \approx 1$ the dynamics is "merely noisy".

To see in more detail how a system with a stable fixed point can give rise to oscillations, consider the dynamics with a large time scale ratio ν. If the dynamics starts away from the fixed point, there is a slow and oscillatory decay towards it, in the course of which the noise repeatedly kicks the system further away from the fixed point which leads to persistent oscillations with a wildly fluctuating amplitude. On the other hand, there is no such effect if the time scale ratio is small: The decay towards the fixed point does not show oscillations visible above the noise level. These issues are further illustrated in Fig. 14.

This behavior is not predicted by the mean-field rate equations of the system. Instead, they have an unstable fixed point associated with a limit cycle with the parameters of the patterned and oscillatory example case, Fig. 7. There are also other approximations that attempt to incorporate the spatial effects or the deviations from full mixing. These include pair approximations [108, 115, 116, 117], phenomenological rescaling of the coordination number of the lattice [118], and treating the finite size of the system as a perturbation [119]. These either are not treating the deviations from full mixing, are considering ensemble averages [119], or fail to predict the dynamics any better than the mean-field approximation does.

In this thesis, a sequence of approximations based on *a posteriori* informa-

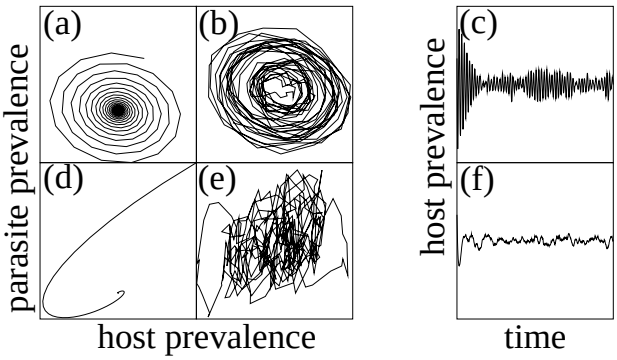

Figure 14: The behavior of Eqs. (41) in the patterned (a, b, c) and in the homogeneous state (d, e, f). The coefficients $a_{\sigma,\sigma'}$ and c_σ are obtained from fits of Eq. (41) to simulation data. In both cases they lead to an oscillatory convergence to the FP (a, d). With noise, the FP is never reached and the cases differ: In the homogeneous one this results in random fluctuations around the FP (e); in the patterned case the noise kicks the system out of the FP with slow and oscillatory decay and leads to persistent oscillations different from limit cycles (b). The host density as a function of time corresponding to (b, e) is shown in (c, f). The parasitoid density (not shown) behaves similarly.

tion drawn from simulations is constructed. These can be considered as corrections on top of the mean-field treatment. The zeroth-order one is to consider the change in the effective values of the spreading rate parameters originating in the spatial effects. Here, one runs simulations, obtains the average host and parasitoid densities and calculates which parameters to insert into the mean-field equations to arrive at the same densities. The parameters so obtained are called here the effective mean-field parameters κ and μ and the procedure above recovers them as a function of the parameters put into the simulations, λ_h and λ_p. The results can be seen in Fig. 15. The change in the parameters caused by the spatial effects appears to be highly nonlinear, hinting to the direction that the spatial effects do more than just trivially rescale the parameters. Furthermore, the boundary between the patterned and non-patterned phases appears also in these considerations and it compares well to the boundary obtained from the domain wall length ratio, Fig. 12.

In the first-order correction, the effective parameters are considered func-

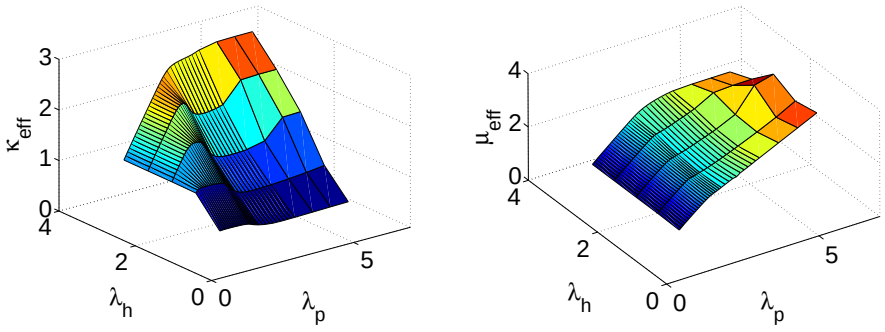

Figure 15: Effective values of the parameters κ (left) and μ (right) as a function of the input parameters λ_h and λ_p.

tions of the instantaneous population densities h_t and p_t. For $\lambda_\alpha I_\alpha(\mathbf{x},t)$ small, they equal the spreading probabilities and the dynamics can be written as

$$h_{t+1} = h_t + \sum_{\mathbf{x}\in\Lambda} \left[\lambda_h k_h(\mathbf{x}) C_{eh}(\mathbf{x},t) - \lambda_p k_p(\mathbf{x}) C_{hp}(\mathbf{x},t)\right] \tag{43}$$

and

$$p_{t+1} = (1-\delta)p_t + \lambda_p \sum_{\mathbf{x}\in\Lambda} k_p(\mathbf{x}) C_{hp}(\mathbf{x},t)\,, \tag{44}$$

where the influence of the connectivities on the prevalence dynamics is expressed in terms of the correlation functions

$$C_{\alpha\beta}(\mathbf{x},t) = \langle \chi_\alpha(\mathbf{x}',t)\chi_\beta(\mathbf{x}+\mathbf{x}',t)\rangle_{\mathbf{x}'}\,. \tag{45}$$

An approximation of these can be written as

$$\begin{aligned} h_{t+1} &= h_t + \kappa(h_t,p_t)\,(1-h_t-p_t)\,h_t - \mu(h_t,p_t)p_t h_t \\ p_{t+1} &= p_t - \delta p_t + \mu(h_t,p_t)p_t h_t\,, \end{aligned} \tag{46}$$

which is of the mean-field form with the interaction parameters $\kappa(h,p)$ and $\mu(h,p)$ generalized to arbitrary functions of the instantaneous densities h and p. To arrive at the first-order correction from here, expand Eqs. (43) and (44) around the fixed point $(\bar{h},\bar{p})$ introducing auxiliary variables η_t and π_t such that $h_t = \bar{h} + \eta_t$ and $p_t = \bar{p} + \pi_t$. One arrives at

$$\begin{pmatrix} \eta_{t+1} \\ \pi_{t+1} \end{pmatrix} = \begin{pmatrix} a_{h,h} & a_{h,p} \\ a_{p,h} & a_{p,p} \end{pmatrix} \begin{pmatrix} \eta_t \\ pi_t \end{pmatrix} \tag{47}$$

with the matrix elements spelled out as

$$\begin{aligned} a_{h,h} &= 1+\kappa-2\kappa\bar{h}-(\kappa+\mu)\bar{p}+\partial_h\kappa\,\bar{h}(1-\bar{h}-\bar{p})-\partial_h\mu\,\bar{h}\bar{p} \\ a_{h,p} &= -(\kappa+\mu)\bar{h}-\partial_p\kappa\,\bar{h}(1-\bar{h}-\bar{p})-\partial_p\mu\,\bar{h}\bar{p} \\ a_{p,h} &= \mu\bar{p}+\partial_h\mu\,\bar{h}\bar{p} \\ a_{p,p} &= 1-\delta+\mu\bar{h}+\partial_p\mu\,\bar{h}\bar{p}\,, \end{aligned} \tag{48}$$

in which μ, κ, their derivatives, and the population densities are evaluated at the fixed point $(\bar{h},\bar{p})$.

If the derivatives in Eq. (48) are zero, Eqs. (47) and (48) fall back to the mean-field approximation, and the matrix in Eq. (47) is the standard linearization matrix of the system. On the other hand, the situation in which the derivatives are nonzero renders the mean-field analysis inapplicable and is interpreted as the instantaneous densities affecting the spreading rates. Since the matrix elements can be measured from the simulations, and everything else is known, one can compute the effective values of the derivatives from the simulations. The results are shown in Fig. 16. Similarly to the effective parameters themselves in Fig. 15, the division between the patterned and non-patterned cases is visible here as well. The derivatives are close to zero in the non-patterned case signalling full mixing and applicability of MF theory whereas they differ crucially from zero in the patterned case corresponding to the failure of the full mixing assumption.

Another straighforward and perhaps more intuitive connection between the amplitude fluctuations is given by considering the system as a set of coupled oscillators. Namely, divide the system into boxes with a mesoscopic size (larger than the typical size of the patterns and smaller than the system size). Now define a phase angle ϕ_i for each oscillator i as the phase angle of the population density inside the box with respect to the average densities, see Fig. 9a. Using these, the degree of synchrony between the boxes is described by the synchronization order parameter [120]

$$r = \frac{1}{N}\Big|\sum_j e^{i\phi_j}\Big|\,, \tag{49}$$

where the summation runs over all N oscillators. The resulting r using a box size of $l \times l = 64 \times 64$ as a function of time is plotted together with the host and parasitoid densities from the same simulation in Fig. 17. The immediate conclusion is that the synchronization order parameter is large

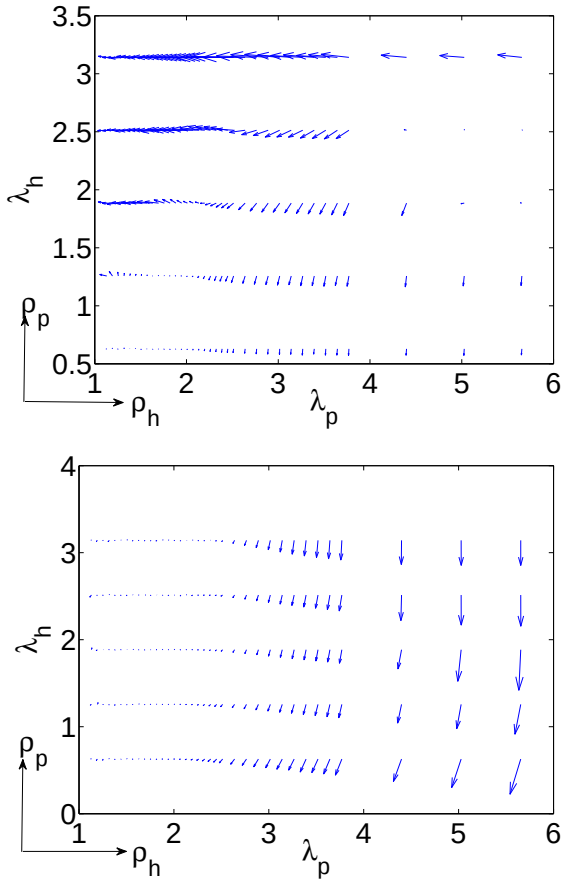

Figure 16: The first-order dependence of the effective parameters on the population densities ρ_h and ρ_p. At each point, the arrow depicts the derivative of κ_{eff} (above) and μ_{eff} (below) according to the auxiliary coordinate system drawn on bottom left. The same points of the parameter space are sampled as in Fig. 15.

exactly when the amplitude is large and vice versa. Therefore, the amplitude fluctuations are interpretable as spontaneous synchronization events of the system at random intervals over at least intermediate length scales.

The model analyzed here on the square lattice is defined in discrete time and discrete space. It also contains an implicit assumption of locally density-dependent establishment. Namely, a given lattice site can be occupied by only one host or parasitoid at a time. Continuous-space treatments do not

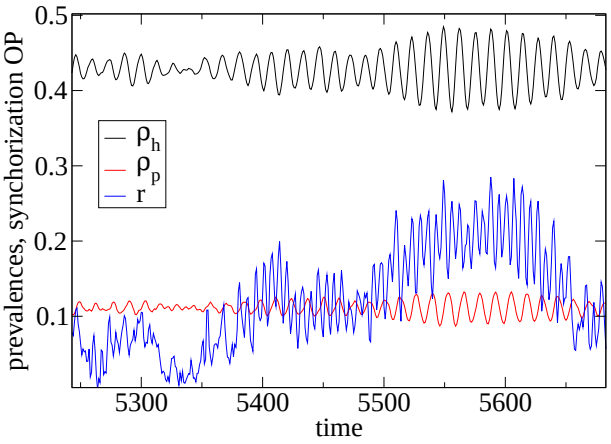

Figure 17: Time series of host and parasite prevalences, and the synchronization order parameter r (Eq. (49)). The parameters are as in Fig. 7. The amplitudes of the oscillations correlate strongly with each other and with the values of r. See Fig. 8 for the dependence of the amplitudes on the system size.

typically have such limitations unless explicitly included. Since in theoretical studies any particular member of this family of eight models can be considered, an interesting question is how does this choice affect the results. Preliminary numerical studies conducted by the author hint to the direction that the choice does not matter in terms of the pattern formation. Note however, that the spreading probabilities above have been chosen such that a straightforward generalization to continuous time does not exist. Studying these issues further is definitely in order in the near future.

3.5 Åland

The empirical metapopulation landscape used as a medium for the host and parasitoid spreading comes from the Åland archipelago in the Baltic Sea between Finland and Sweden. The archipelago itself consists of thousands of islands, some of which are even smaller than 100 m, whereas the biggest one is about 30 km in diameter. Around 4000 meadows acting as distinct habitat patches of the Glanville fritillary butterfly *Melitaea cinxia* have been located in spatial coordinates and their areas have been measured [69, 100, 121]. The patches themselves are not distributed according to a

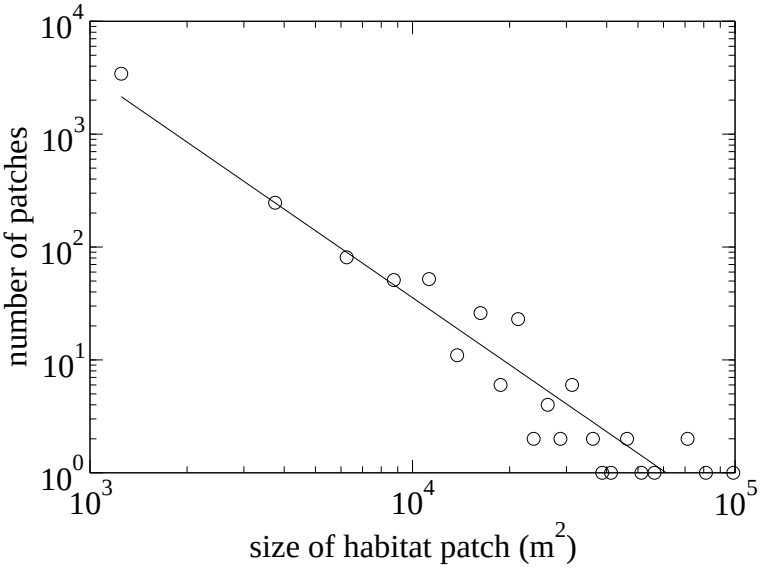

Figure 18: Number of patches as a function of patch sizes in the empirical Åland metapopulation landscape. The solid line is a guide to the eye and indicates a $1/A^2$-behavior.

uniformly random process but they are instead highly clustered. Similarly, the patch areas A are distributed according to a broad distribution with roughly a power-law decay $P \sim A^{-2}$ for the probability P that a randomly chosen patch has area A. The measured distribution is shown in Fig. 18.

The Åland landscape can be mapped to a graph to both obtain knowledge about its structure and to facilitate using the SIS model and the host–parasitoid model on graphs. Here, this is done via considering the possible intensity of immigrants to patch i due to emigrants from patch j. Define a *migration kernel*

$$f_{ij} = C A_i^\beta A_j^\beta \exp(-r_{ij}/D)\,, \tag{50}$$

(cf. Eq. (13)) where C is a constant prefactor, A_i's are the patch areas, β and D are parameters, and r_{ij} is the distance between patches i and j. Using this, a graph is formed out of the set of patches so that two of them, j and k are connected with an edge if the condition $f_{jk} > T$, where T is a predefined threshold, is fulfilled. The graphs so formed can take a variety of forms, depending on the parameters. Here, two qualitatively different kinds of graphs in terms of the degree distribution are obtained, a power-law graph and one with an exponential degree distribution. See Fig. 19 for examples

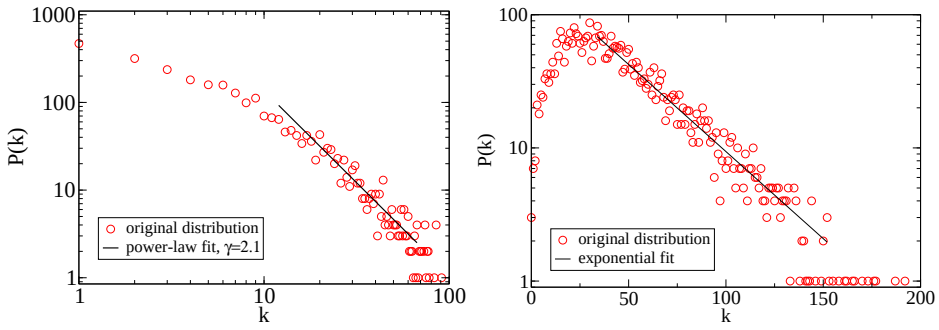

Figure 19: Example degree distributions of the graphs created from the empirical Åland metapopulation landscape corresponding to power-law graphs (on the left) and exponential degree distributions (on the right).

and article **II** for the parameters. The Åland graph is naturally highly clustered for any parameters, and also exhibits degree–degree correlations such that the average nearest-neighbour degree can be approximated as $\bar{k}_{nn}(k) \sim k^{1/2}$. Also, there are positive correlations between the degree of a given patch and its area.

In addition to forming a graph out of the Åland landscape, it can be considered as such and the host–parasitoid model with connectivity-driven spreading for both species defined in Section 3.1 becomes directly applicable. In this thesis a variant of the model where the contribution of each patch to the connectivities is multiplied by its area and in addition to the connectivity-driven spreading a small amount of uniformly random reproduction is used. Both differences are biologically motivated, since the immigration pressure from a given patch increases with the local population which in turn increases with the area of the patch supporting it, and random spreading mimicks occasional long-range dispersal. A snapshot of the system simulated in this way is shown in Fig. 20 together with the corresponding time series in the inset.

The observations from the simulations of this case are rather similar to those made on regular square lattices in Section 3.4. Namely, the patterning is clearly there, and the domain structure is analogous to that in the square lattice case. In addition, the dynamics of the system shows erratic oscillations, and the analysis of Section 3.4.2 can be repeated here, revealing noise-sustained oscillations. More detailed studies of the model on the Åland landscape are suggested for the future. Such research includes, among other

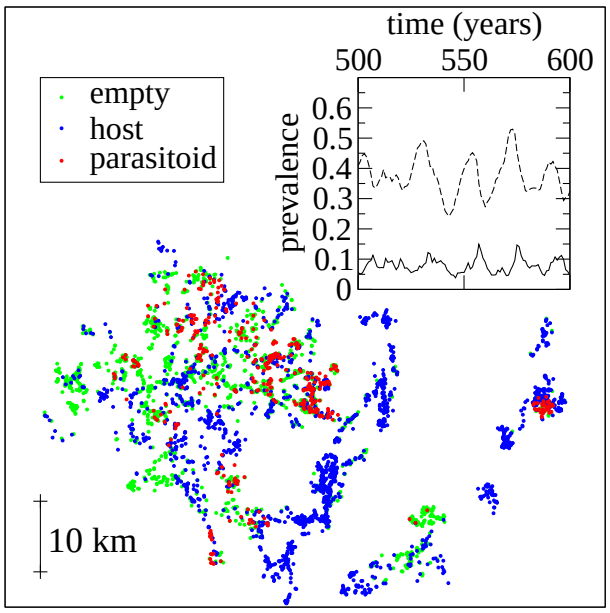

Figure 20: Main figure: a snapshot of the simulated dynamics of hosts and parasitoids on the Åland patch geometry. Each dot corresponds to a single patch. Inset: the prevalence of the hosts (dashed line) and parasitoids (solid line) as a function of time. As spreading widths we have used $w_h = 1000$ m and $w_p = 500$ m. The annual death probability is $\delta = 0.9$ and the host and parasitoid spreading rate parameters are $\lambda_h = 100$ and $\lambda_p = 1400$. A fraction of 0.01 of the hosts spreads randomly to all patches. The archipelago is roughly 60 km $\times$ 80 km in size.

issues, systematically considering the effect of all the parameters. Also, the effect of the landscape should be studied, for example by comparing the results on the empirical landscape to the same at a homogeneous but not necessarily regular landscape with the same average distance between the nodes. A family of interesting cases would also be given by interpolating between a homogeneous landscape and an inhomogeneus one with the same characteristics as the Åland landscape.

4 Rock–paper–scissors games

In this Section, the rock–paper–scissors game is studied. In particular, the effect of the conservation law of the total density of the three populations on pattern formation and extinction transitions is under scrutiny, together with the effect of rate asymmetry. The results discussed in this Section have been published in article **VI**.

4.1 Models

The rock–paper–scissors games in general deal with cyclic dominance of three species, A, B and C, and its classical three-state version is defined by the following reaction equations and corresponding rates:

$$\begin{array}{l} AB \to AA \quad \text{with rate } \mu\,, \\ BC \to BB \quad \text{with rate } \mu\,, \\ CA \to CC \quad \text{with rate } \mu\,. \end{array} \tag{51}$$

In the mean-field approximation, the rate equations corresponding to the reaction equations above are

$$\begin{array}{l} \partial_t a = \mu ab - \mu ac\,, \\ \partial_t b = \mu bc - \mu ab\,, \\ \partial_t c = \mu ca - \mu cb\,, \end{array} \tag{52}$$

where a, b, and c are densities of the states A, B, and C, respectively. The fixed point $a = b = c = \frac{1}{3}$ of these equations is marginally stable, which in finite populations leads always to extinction at the long-time limit [78]. However according to numerical studies, the two-dimensional fully spatial counterpart of the three-state RPS game is known to have a stable fixed point, reproduced by a four-site approximation [76].

A variant of the RPS game considering empty space in addition to the three different states has been recently proposed [37]. It is described by the following rate equations

$$\begin{array}{lcll} AB & \to & EA & \text{with rate } \sigma, \\ BC & \to & EB & \text{with rate } \sigma, \\ CA & \to & EC & \text{with rate } \sigma, \\ XE & \to & XX & \text{with rate } \mu, \end{array} \tag{53}$$

where X can refer to any state, E denotes empty space, and A, B, and C are as above. The corresponding rate equations are [38]

$$\begin{aligned} \partial_t a &= a[\mu(1-\rho) - \sigma c] \,, \\ \partial_t b &= b[\mu(1-\rho) - \sigma a] \,, \\ \partial_t c &= c[\mu(1-\rho) - \sigma b] \,, \end{aligned} \tag{54}$$

where $\rho = a + b + c$ is the total density. These equations have a reactive linearly unstable fixed point for all μ and σ [38]

$$a = b = c = \frac{\mu}{3\mu + \sigma} \,. \tag{55}$$

The difference between the three- and the four-state formulations is not purely microscopic: In the three-state version the total density $\rho = a + b + c = 1$ is conserved whereas in the four-state case it becomes an aggregate of the basic dynamical variables of the system. Both versions of the model can be amended with an exchange reaction

$$XY \to YX \quad \text{with rate} \quad D \,, \tag{56}$$

where X and Y can denote any state (including empty space), and D is a diffusion constant.

It has been shown recently [37, 38] that in the four-state formulation with two spatial dimensions and diffusion the system forms spiral-shaped patterns that grow as a function of the diffusion constant. When the wave length of the spirals grows to be of the same order of magnitude than the system size, there is a transition from reactive coexistence to extinction of two species. In this thesis, two issues related to this are investigated. The first one asks if there is a similar transition in the three-state model as well, i.e. if explicit handling of the empty space is important in this context. The latter considers the effect of a small asymmetry in the reaction rates on both the transition and the spiral pattern formation.

4.2 Conservation of total density

The spatial four-state RPS game defined by Eqs. (54) and (56) has been recently approximatively mapped [38] to the complex Ginburg-Landau equation by exploiting the instability of the fixed point in Eq. (55). The mapping

proceeds as follows. First, the reactive fixed point is shifted to the origin. Then, the rate equations are expanded around it to find an attractive two-dimensional invariant manifold, the dynamics is expressed on the manifold, and a normal-form transformation is performed. In it, a quadratic transformation whose linear terms form the identity mapping is searched such that the resulting time-development equations for the dynamical variables have no quadratic term. In the four-state case, the resulting equations are up to third order [38]

$$\begin{aligned} \partial_t z_A &= c_1 z_A + \omega z_B - c_2(z_A + c_3 z_B)(z_A^2 + z_B^2)\,, \\ \partial_t z_B &= c_1 z_B - \omega z_A - c_2(z_B - c_3 z_A)(z_A^2 + z_B^2)\,, \end{aligned} \tag{57}$$

where z_A and z_B parametrize the invariant manifold,

$$\omega = \frac{\sqrt{3}}{2}\frac{\mu\sigma}{3\mu+\sigma}\,, \tag{58}$$

$$c_1 = \frac{1}{2}\frac{\mu\sigma}{3\mu+\sigma}\,, \tag{59}$$

$$c_2 = \frac{\sigma(3\mu+\sigma)(48\mu+11\sigma)}{56\mu(3\mu+2\sigma)}\,, \tag{60}$$

and

$$c_3 = \frac{\sqrt{3}(18\mu+5\sigma)}{48\mu+11\sigma}\,. \tag{61}$$

This is to be compared with the standard form of the CGLE [54]

$$\partial_t z = z + (1+ib)\Delta z - (1+ic)|z|^2 z\,, \tag{62}$$

where the complex variable z is $z = z_A + iz_B$, to see the direct correspondence and to be able to compare the parameters.

In this thesis, a similar calculation is carried out for the three-state case. It is somewhat simpler since there are two independent dynamical variables to begin with and the phase space spanned by them can be regarded as the counterpart of the invariant manifold above. The resulting rate equations are

$$\begin{aligned} \partial_t z_A &= \omega z_B + c_2 z_A^2 z_B + c_2 z_B^3\,, \\ \partial_t z_B &= -\omega z_A - c_2 z_A^3 - c_2 z_A z_B^2\,, \end{aligned} \tag{63}$$

where $\omega = \frac{\sqrt{3}}{3}$ and $c_2 = -\frac{\sqrt{3}}{2}$. Writing this in a form as closely resembling the CGLE as possible adding diffusion in the process as above one arrives at

$$\partial_t z = i\omega z + D\Delta z + ic_2|z|^2 z\,. \tag{64}$$

Further, changing to a rotating coordinate system (replace z by $ze^{i\omega t}$) removes the purely imaginary linear term, and the resulting equation reads

$$\partial_t z = D\Delta z + ic_2|z|^2 z\,. \tag{65}$$

When comparing this to the CGLE, Eq. (62), one sees that there is a crucial difference: The linear term is absent here. When following the calculation, it is apparent that this is a direct consequence of the marginal stability of the corresponding fully-mixed rate equations.

To see how the presence or absence of the linear term affects the situation, substitute a generic single-spiral solution [54]

$$z = a(r)e^{i[\omega t \pm \phi + \psi(r)]}\,, \tag{66}$$

where $a(r)$ and $\psi(r)$ are real functions and r and ϕ are the spatial coordinates in the cylindrical coordinate system, to the equations with and without the linear term. The conclusion is that the spiral solution with a finite wave length exists only if the linear term is present. In other words, this calculation predicts that the three-state RPS game does not support spiral-forming solutions. The same argument can be made using the plane-wave solution as well with the same conclusion.

Numerical simulations of the model on a regular lattice of size $L \times L$ is rather straightforward. In them, for each microscopic time step, a process (selection, reproduction, or diffusion) is chosen randomly with probabilities proportional to the rates, a random lattice site and its random neighbour is selected at random, and the reaction is executed if allowed by the rules. The time is increased by $\delta t = 1/(\tau L^2)$ where τ is the sum of the rates. To speed up the simulation in case the reaction rates are vastly different, an algorithm by Gillespie [122, 123] could be used but it has not been implemented here.

The prediction above is confirmed by numerical simulations. Fig. 21 shows example configurations created by the system in both the three-state and the four-state formulation. In the four-state case, spirals form, reproducing the results in [37, 38, 124], and in the three-state case there are indeed no spirals. However, the three-state case also has an emergent length scale comparable to the spiral wave length of the four-state case. Applying an argument previously used in the context of the contact process with diffusion [105, 125, 126], the length scale is given by the diffusion-induced correlation length as follows. Consider a homogeneous system in its steady state with a small spatially localized perturbation caused by noise. If its typical lifetime

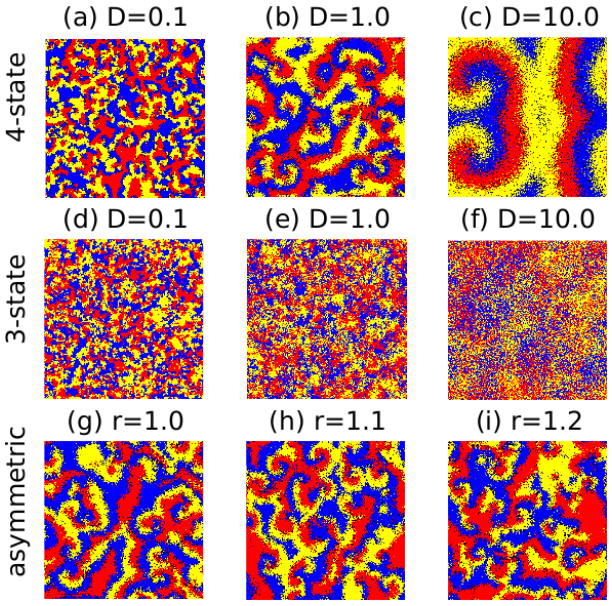

Figure 21: Example runs of the RPS game in a lattice of size $L \times L = 200$. (a), (b) and (c): the four-state model with different diffusion constants and $\mu = \sigma = 1$. (d), (e), (f): the three-state model with different diffusion constants and $\mu = 1$. (g), (h), (i): the rate-asymmetric four-state model with different asymmetries $r = 1 + \epsilon$, $D = \mu = \sigma = 1.0$.

is t_d, it diffuses up to distance $x = \sqrt{2Dt_d}$ before decaying. Thus, the correlation length becomes of the order of the system size when

$$\frac{D}{L^2} = \frac{1}{2t_d} \tag{67}$$

and a cross-over to extinction should take place as the diffusion constant exceeds this value. In other words, the spiral pattern formation is not a necessary condition for the crossover to extinction. The time scale t_d in the equation above can be numerically estimated as the characteristic time of the autocorrelation function of the global densities.

Fig. 22 shows the extinction probability in long simulations for both the four- and three-state models as a function of the diffusion constant. It is seen that the scaling $D_c \propto L^2$ for the value of the diffusion constant at the crossover to extinction indeed holds, and the numerical prediction for this value, Eq. (67), is also in good agreement with the simulations. Note

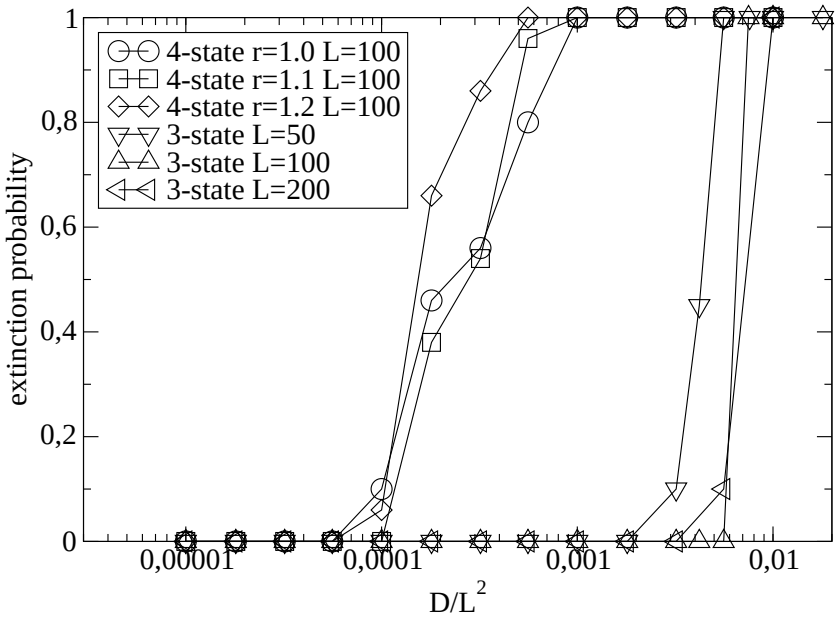

Figure 22: The extinction probability as a function of the scaled diffusion constant D/L^2 in various cases in the RPS game. For both the three- and the four-state models there is a crossover to an absorbing state with two of the three subpopulations extinct. The location of this crossover scales as $D_c \propto L^2$ in both cases and in the four-state case the introduction of rate asymmetry does not affect the location of the crossover for small asymmetries.

however that paying attention to the details is in order, if quantitative predictions are to be made: The value of the diffusion constant at which the coexistence is destroyed by the extinction can differ by more than an order of magnitude for the two cases considered here.

4.3 Rate asymmetry

Almost all theoretical studies so far (with the notable exception of [127]) have assumed that the microscopic processes are rate-symmetric. In other words, one can cyclically permute the three species without any change whatsoever. However, experiments can both simultaneously show the formation of spirals [72], and still be built such that the detailed pairwise

reaction mechanisms are different for different pairs of species [73]. It is apparent that a small asymmetry in the reaction rates does not destroy the spirals.

To study this issue in the four-state RPS game, a rate-asymmetric variant of it is introduced in this thesis as

$$\begin{array}{rcll} AB & \to & AE & \text{with rate } \sigma\,, \\ BC & \to & BE & \text{with rate } \sigma\,, \\ CA & \to & CE & \text{with rate } \sigma\,, \\ AE & \to & AA & \text{with rate } \mu\,, \\ BE & \to & BB & \text{with rate } \mu\,, \\ CE & \to & CC & \text{with rate } r\mu\,, \\ XY & \to & YX & \text{with rate } D\,, \end{array} \tag{68}$$

where $r = 1 + \epsilon$ ($\epsilon > 0$) is assumed to be close to one, and X and Y can refer to any state including the empty space E. This is the simplest possible extension of the original four-state model that incorporates rate asymmetry. The corresponding MF rate equations are

$$\begin{aligned} \partial_t a &= a[\mu(1-\rho) - \sigma c]\,, \\ \partial_t b &= b[\mu(1-\rho) - \sigma a]\,, \\ \partial_t c &= c[r\mu(1-\rho) - \sigma b]\,. \end{aligned} \tag{69}$$

These have the reactive fixed point

$$a = c = \frac{\mu}{(2+r)\mu + \sigma}\,;\; b = \frac{r\mu}{(2+r)\mu + \sigma}\,. \tag{70}$$

From the rate equations (69) one can in principle follow the calculation of [38] for small ϵ by first expressing the change in the orientation of the invariant manifold up to first order in ϵ, and subsequently finding the normal form at the same limit. While this procedure is possible by brute force, which has been certified here by carrying it out, the resulting expressions get rather heavy and do not appear to be useful for gaining physical intuition. Instead, one can argue that the resulting normal-form equation amended with diffusion is always the one at $\epsilon = 0$ [38]

$$\partial_t z = c_1 z + D\Delta z - c_2(1 + ic_3)|z|^2 z\,, \tag{71}$$

to which the most general leading order correction from rate asymmetry,

$$\partial_t z = ... + \epsilon(d_1 z_A^3 + d_2 z_A^2 z_B + d_3 z_A z_B^2 + d_4 z_B^3)$$

$$+i\epsilon(d_5 z_A^3 + d_6 z_A^2 z_B + d_7 z_A z_B^2 + d_8 z_B^3)\,, \tag{72}$$

where the ellipsis stands for the non perturbed terms in Eq. (71), has to be added. Let us now express this in polar coordinates. Write the phase-space coordinates as $z = Re^{i\theta}$ and the position-space coordinates as (r, ϕ). Now, Eqs. (71) and (72) are

$$\partial_t R = c_1 R + D(\Delta R - R(\nabla\theta)^2) - c_2 R^3 + \epsilon R^3 f(\theta) \tag{73}$$

$$R\partial_t\theta = D(2\nabla\theta\cdot\nabla R + R\Delta\theta) - c_2 c_3 R^3 + \epsilon R^3 g(\theta)\,, \tag{74}$$

where f and g are smooth 2π-periodic functions with the property that their Fourier series do not have a constant term and have only a finite number of higher-order terms.

To arrive at a solution to the perturbed equations similar to the standard single-spiral solution, Eq. (66), one has to find the change of variables that reverses the perturbation up to the first order in ϵ. Such a change of variables has to be of the form

$$R = \tilde{R}[1 + \epsilon h(\theta)]\,, \tag{75}$$

with the function $h(\theta)$ to be determined. It has been shown that the correct choice for $h(\theta)$ is

$$h(\theta) = \frac{F_0^2}{2q^2} f(\theta)\,, \tag{76}$$

where F_0 is the limiting value of R at the limit $r \to \infty$. So, the perturbed system has a single-spiral solution where the oscillation amplitude has an additional phase-dependent prefactor essentially cancelling out the perturbation at linear order. Since the average of $f(\theta)$ over θ vanishes, a small change of variables does not alter the average spiral wave length, and therefore also not the location of the crossover to extinction. The resulting system is still essentially the CGLE only after an unimportant (in the first order) change of variables. As a result, rate-symmetric theory and rate-asymmetric experiments are comparable.

These results have also been confirmed numerically. First, panels (g), (h), and (i) of Fig. 21 show example states of the four-state RPS game with different values of r. A visual inspection hints that even though the appearance of the patterns changes somewhat, they can still be considered spirals and that the average wave length remains roughly the same. Also the extinction probability as a function of the diffusion constant shown in Fig. 22 for several values of r confirms these findings: The location of the crossover does not change.

5 Conclusion

This thesis consists of studies of statistical mechanics of various systems. First, bipartite collaboration networks formed of social actors and social ties are studied. Empirical measurements of such networks indicate that in the one-mode projection onto the social actors, the degree distributions have fat tails, although they are not necessarily literally power laws. Also substantial clustering is observed together with assortative mixing, both well-known signatures of large social networks. The assortative mixing shows up not only in the assortativity coefficient but also in the average nearest-neighbour degree (ANND) $\bar{k}_{nn}(k)$ as a function of the node degree k. Namely, $\bar{k}_{nn}(k) \propto k^{\alpha}$ with $\alpha \approx 0.3$ for all networks considered. The empirical results for the one-mode projection onto the social ties are qualitatively similar. A new numerical model for the growth of such networks through the addition of one social tie at a time is introduced, and compared to the empirical observations and predictions from earlier models. The most important ingredient of the new model is the incorporation of a sublinear preferential attachment rule. It, together with earlier models, is shown to agree with the empirics in some measures while failing to reproduce reality in several others.

These shortcomings highlight the need for more developed treatments of the issue. Most importantly, a numerical model reproducing both sublinear preferential attachment and a power-law ANND still appears to be missing. This is emphasized further by the fact that new models of such networks ([94], for instance) have been introduced recently, and that new examples of empirical collaboration networks (e.g. [92]) keep appearing in the literature. Candidate models need to implement a simple growth rule that measures the structure of the network in a way that captures the essence of the selection of coauthors for scientific publications in a statistical sense. The sublinear coupling of the selection rule to the degrees of the node then can be either a building block of the rule or – more likely – a consequence of a growth rule that is not explicitly coupled to the degree. A large family of such rules can be constructed by letting the attachment probabilities be proportional to any node-specific time-dependent scalar (or the same to some power α). Such rules are readily implementable and choices for the scalar replacing the degree are numerous. One interesting example is given by the betweenness centrality [98], and studies using these ideas are suggested for the future.

Second, population dynamics of a model of two populations, host and parasitoids, is studied in several environments. On Bethe lattices, the phase

diagram of the model showing the transitions to extinction corresponding to both species respectively is derived analytically via various approximations, and roughly constructed from numerical simulations. The most crucial property of the phase diagram is the lack of a tricritical point: There is no transition boundary separating the regions with both populations alive and both extinct. While not directly applicable to any empirical systems, this case still has interest as an analytically tractable special case.

The behavior of the parasitoids on scalefree graphs is shown to be similar to the behavior of the hosts were they living on the graph by themselves without any parasitoids. In other words, they are comparable to the infected nodes in the SIS model. As a consequence, earlier well-known results on the absence of a critical threshold for the hosts [102, 109] are directly generalizable also for the parasitoids in this two-species model. Simply put, at the thermodynamic limit, both populations are expected to be alive in the whole two-dimensional parameter space of the spreading rates, if the second moment of the degree distribution of the underlying network diverges, as is the case for power-law degree distributions $P(k) \sim k^{-\gamma}$ for $\gamma \leq 3$·

A similar model with spreading not restricted to nearest neighbours on a graph or a lattice has been studied here on regular square lattices. In them in a certain region of the parameter space, the model leads to persistent oscillations coupled with the build-up of strong spatial correlations showing up as highly irregular noisy spirals. The oscillations are shown not to conform to the classical limit cycle picture, have an erratically fluctuating amplitude, and are given an explanation as a consequence of a time scale separation and noise. Hence, they are called noise-sustained oscillations. This is in contrast to the corresponding mean-field theory yielding classical limit cycles. The results obtained here serve, among other things, as a warning that in a system with limit cycle oscillations in the mean-field and observed oscillations in full spatial simulations, the extended case might not conform to the limit cycle picture. The type of the oscillations is relevant for the population stability, for instance. Namely, the vulnerability of the system to extinction can depend on the fluctuation level of the amplitude, which in turn depends strongly on the particular mechanism of the oscillations. Therefore, it might be worthwhile to check for the possibility of noise-sustained oscillations in several cases. Potential candidates include [27, 115, 116, 117, 128].

The observations also merit some further discussion. First, the structure of the phase diagrams and the existence of the oscillations depend on the par-

ticular interaction paradigm chosen. Different reaction schemes can lead to different behavior even when they describe two competing biological species, as exemplified by [129]. Second, the dispersal might take place in Levy flights, in which case the the dispersal kernel controlling the spreading does not have a well-defined length scale like the exponential kernel used in this work. Here, a naïve expectation is that the behavior will be more mean-field-like, i.e. the oscillations will be more stable, but comprehensive numerical studies of these issues are definitely in order in the future. Third, seeing the oscillatory behavior associated with the formation of the erratic spirals does in practice require longer spreading lengths than one lattice spacing. This is because the spiral wave length is proportional to the characteristic spreading length, and the former needs to be long enough not to get lost under the graininess of the lattice.

A comparison to earlier results [130] stating that temporally periodic phases cannot be stable in two dimensions in a class of domain-growth models is also in order. The present results are not in contradiction with these claims for two reasons. First, the statement of [130] holds only for continuous-time systems whereas here a discrete-time one is dealt with. Second, more importantly, the oscillations recovered here are not stable in the usual sense: There is no long-range order associated with them, and no long-time autocorrelation.

The spatial patterns are characterized by a vast array of methods introduced here. These measurements show that the parameter space is divided into regions with and without spatial patterns. The division is a continous crossover with no qualitative change in the behavior: The region with no patterns can be described as one in which they are strongly suppressed. The patterning is coupled to the dynamics by showing that it leads to a dependence of the reaction rates on the instantaneous population densities, which in turn leads to the noise-sustained oscillations. In other words, the particular type of the oscillations is shown to originate in the spatial correlations.

The host–parasitoid model with distance-dependent spreading is also simulated on a two-dimensional metapopulation landscape that has been measured empirically [70, 71]. In this case, the general conclusion is that while the features of the regular square lattice are qualitatively transferred to the empirical case as well, the effect of the irregularity is to further stabilize the dynamics with respect to that on the regular lattice. This is of interest since the expectation for densely connected systems – such as the example

landscape – is to be close to the mean-field behavior whereas the opposite is observed here in the simulations. It would be of interest to study the effect of the landscape on the dynamics by, for example, comparing the dynamics on a homogeneous but not necessarily regular landscape to that on the empirical landscape. Also other empirical landscapes call for similar simulations, should such become available.

Finally, rock–paper–scissors games corresponding to cyclic dominance of three species is studied in two spatial dimensions with diffusion. Previous works [37] have shown that in a four-state formulation of the game spatial patterns, spirals, form and that there is a crossover from the coexistence of all three species to extinction of two of them as a function of the diffusion constant. Namely, the spiral wave length increases with the diffusion constant and once it becomes of the order of system size, the behavior is essentially fully mixed, which in turn has been previously shown to lead to eventual extinction [78]. The work done here extends the earlier studies by answering two questions. First, it is studied whether the spiral formation and the crossover to extinction also take place in a three-state formulation of the game not taking empty space explicitly into account. The second question asks what is the effect of a small rate asymmetry in the four-state formulation, i.e. what happens if the three species do not obey cyclic permutation symmetry.

In it shown here that in the three-state model spirals do not form: The resulting spatial configurations can be called homogeneous. However, the existence of an emergent length scale, a correlation length, arising from stochasticity and diffusion is demonstrated, and that the lenght scale also increases with the diffusion constant. Consequently, there is a similar crossover to extinction once this length outgrows the system size. In other words, even though the spiral formation can lead to extinction in RPS games, it is not a necessary ingredient since length scales not as clearly visible as a spiral wave length can still emerge with similar consequences. However, the location of the crossover differs more than an order of magnitude between the cases, and therefore being able to pinpoint the mechanism behind the extinction remains important.

It is also shown that a small rate asymmetry in the reaction rates does not destroy the spirals in the four-state formulation. Furthermore, it does not even alter the average wave length of them in the first order, and therefore it does not have an effect on the location of the crossover to extinction. This result serves as a partial explanation to why spirals still form in experiments

of systems of three strains of bacteria [72] even though such experiments can be constructed such that no permutation symmetry for the reaction rates exists [73]. The behavior of the RPS game under large asymmetries in the reaction rates remains an open question, which is fortunately amenable to numerical studies at least. A recent study of a non-spatial three-state game with rate asymmetry [127] paves the way to this direction.

References

[1] M. Kardar, *Statistical Physics of Particles*, (Cambridge University Press, Cambridge, 2007).

[2] R. K. Merton, Science **159**, 56 (1968).

[3] C. Castellano, S. Fortunato, and V. Loreto, e-print, arXiv/0710.3256.

[4] R. N. Mantegna, and H. E. Stanley, *An Introduction to Econophysics: Correlations and Complexity in Finance*, (Cambridge University Press, Cambridge, 1999).

[5] R. Albert and A.-L. Barabási, Rev. Mod. Phys. **74**, 47 (2002).

[6] S. N. Dorogovtsev and J. F. F. Mendes, Adv. Phys. **51**, 1079 (2002).

[7] M. E. J. Newman, SIAM Rev. **45**, 167 (2003).

[8] S. N. Dorogovtsev and J. F. F. Mendes, *Evolution of Networks: From Biological Nets to the Internet and WWW*, (Oxford University Press, Oxford, 2003).

[9] R. Pastor-Satorras and A. Vespignani, *Evolution and Structure of the Internet: A Statistical Physics Approach*, (Cambridge University Press, Cambridge, 2004).

[10] S. N. Dorogovtsev, A. V. Goltsev, and J. F. F. Mendes, Rev. Mod. Phys. **80**, 1275 (2008).

[11] D. J. Watts, *The Science of a Connected Age*, (Norton, New York, 2003).

[12] A.-L. Barabási and R. Albert, Science **286**, 509 (1999).

[13] S. N. Dorogovtsev, J. F. F. Mendes, and A. N. Samukhin, Phys. Rev. Lett **85**, 4633 (2000).

[14] S. N. Dorogovtsev and J. F. F. Mendes, Phys. Rev. E **62**, 1842 (2000).

[15] P. L. Krapivsky, S. Redner, and F. Leyvraz, Phys. Rev. Lett. **85**, 4629 (2000).

[16] P. L. Krapivsky and S. Redner, Phys. Rev. E **63**, 066123 (2001).

[17] P. Holme and B. J. Kim, Phys. Rev. E **65**, 026107 (2002).

[18] G. Galdarelli, A. Capocci, P. de los Rios, and M. A. Muñoz, Phys. Rev. Lett. **89**, 258702 (2002).

[19] A. J. Lotka, *Elements of Physical Biology*, (Williams and Wilkins, Baltimore, 1925).

[20] V. Volterra, Atti R. Accad. Naz. Lincei, Mem. Cl. Sci. Fis., Mat. Nat. **2**, 31 (1926).

[21] M. P. Hassell, H. N. Comins, and R. M. May, Nature **353**, 255 (1991).

[22] H. N. Comins, M. P. Hassell, and R. M. May, J. Anim. Ecol. **61**, 735 (1992).

[23] A. T. Bradshaw and L. L. Moseley, Physica A **261**, 107 (1998).

[24] B. Blasius, A. Huppert, and L. Stone, Nature **399**, 354 (1999).

[25] A. F. Rozenfeld and E. V. Albano, Physica A **266**, 322 (1999).

[26] M. Droz and A. Pekalski, Phys. Rev. E **63**, 051909 (2001).

[27] T. Antal and M. Droz, Phys. Rev. E **63**, 056119 (2001).

[28] R. V. Solé and J. Bascompte, *Self-Organization in Complex Ecosystems*, (Princeton University Press, Princeton, 2006).

[29] D. Tilman, R. M. May, C. L. Lehman, and M. A. Nowak, Nature **371**, 65 (2002).

[30] I. Hanski and O. Ovaskainen, Cons. Biol. **16**, 666 (2002).

[31] K.-i. Tainaka, Phys. Rev. E **50**, 3401 (1994).

[32] M. Pascual, M. Roy, F. Guichard, and G. Flierl, Phil. Trans. Roy. Soc. Lond. B **357**, 657 (2002).

[33] F. Zhang, Z. Li, and C. Hui, Ecol. Modell. **193**, 721 (2006).

[34] M. Mobilia, I. T. Georgiev, and U. C. Täuber, J. Stat. Phys. **128**, 447 (2007).

[35] W. S. C. Gurney, A. R. Veitch, I. Cruickshank, and G. McGeachin, Ecology **79**, 2516 (1998).

[36] T. Nguyen-Huu, C. Lett, J. C. Poggiale, and P. Auger, Ecol. Modell. **197**, 290 (2006).

[37] T. Reichenbach, M. Mobilia, and E. Frey, Nature **448**, 1046 (2007).

[38] T. Reichenbach, M. Mobilia, and E. Frey, J. Theor. Biol. **251**, 368 (2008).

[39] G. Szabó, A. Szolnoki, T. Antal, and I. Borsos, Phys. Rev. E **55**, 5257 (1997).

[40] G. Szabó, M. A. Santos, and J. F. F. Mendes, Phys. Rev. E **60**, 3776 (1999).

[41] G. Szabó and A. Szolnoki, Phys. Rev. E **65**, 036115 (2002).

[42] G. A. Tsekouras and A. Provata, Phys. Rev. E **65**, 016204 (2002).

[43] A. Provata and G. A. Tsekouras, Phys. Rev. E **67**, 056602 (2003).

[44] A. Szolnoki, G. Szabó, and M. Ravasz, Phys. Rev. E **71**, 027102 (2005).

[45] R. Imbihl and G. Ertl, Chem. Rev. **95**, 697 (1995).

[46] E. V. Albano, Phys. Rev. E **57**, 6840 (1998).

[47] V. P. Zhdanov, Phys. Rev. E **59**, 6292 (1999).

[48] V. P. Zhdanov, Physica D **144**, 87 (2000).

[49] T. Lele and J. Lauterbach, Chaos **12**, 164 (2002).

[50] V. P. Zhdanov, Surf. Sci. Rep. **45**, 231 (2002).

[51] D. E. Clapham, Cell **80**, 259 (1995).

[52] M. J. Berridge, J. Physiol. **299**, 291 (1997).

[53] M. Falcke, Adv. Phys. **53**, 255 (2004).

[54] I. S. Aranson and L. Kramer, Rev. Mod. Phys. **74**, 99 (2002).

[55] X. Lambin, D. A. Elston, S. J. Petty, and J. L. MacKinnon, Proc. Roy. Soc. Lond. B **265**, 1491 (1998).

[56] J. van de Koppel, M. Rietkerk, N. Dankers, and P. M. J. Herrman, Am. Nat. **165**, E66 (2005).

[57] E. Ranta and V. Kaitala, Nature **390**, 456 (1997).

[58] I. Hanski, H. Henttonen, E. Korpimäki, L. Oksanen, and P. Turchin, Ecology **82**, 1505 (2001).

[59] J. van de Koppel. J. C. Cascoigne, G. Theraulaz, M. Rietkerk, W. M. Mooij, and P. M. J. Herrman, Science **322**, 739 (2008).

[60] *Metapopulation Biology*, edited by I. Hanski and M. E. Gilpin (Academic Press, San Diego, 1997).

[61] I. Hanski, Nature **396**, 41 (1998).

[62] W. S. Lahaye, R. J. Gutierrez, and H. Resit Ackakaya, J. Anim. Ecol. **63**, 775 (1994).

[63] J. F. ter Braak, I. Hanski, and J. Verboom, in *Modelling Spatiotemporal Dynamics in Ecology*, eds. J. Bascompte and R. V. Solé (Springer, New York, 1998).

[64] H. Resit Akcakaya and B. Baur, Oecologia **105**, 475 (1996).

[65] W. Stewart, J. F. Dallas, S. B. Piertney, F. Marshall, S. Telfer, A. Sharul, and X. Lambin, Biol. J. Linn. Soc. **68**, 159 (1999).

[66] A. Moilanen, A. T. Smith, and I. Hanski, Am. Nat. **152**, 530 (1998).

[67] S. D. W. Frost, M.-J. Dumaurier, S. Wain-Hobson, and A. J. Leigh Brown, Proc. Natl. Acad. Sci. USA **98**, 6875 (2001).

[68] J. Keymer, P. Galadja, C. Muldoon, S. Park, and R. H. Austin, Proc. Natl. Acad. Sci USA **103**, 17290 (2006).

[69] I. Hanski, J. Anim. Ecol **63**, 151 (1994).

[70] S. van Nouhuys and I. Hanski, J. Anim. Ecol. **71**, 639 (2002).

[71] S. van Nouhuys and I. Hanski, in *On the Wings of Checkerspots: A Model System for Population Biology*, eds. P. R. Erlich and I. Hanski (Oxford University Press, Oxford, 2004).

[72] B. Kerr, M. A. Riley, M. W. Feldman, and B. J. M. Bohannan, Nature **418**, 171 (2002).

[73] M. Loose, E. Fischer-Friedrich, J. Ries, K. Kruse, and P. Schwille, Science **320**, 789 (2008).

[74] B. Sinervo and C. M. Lively, Nature **380**, 240 (1996).

[75] B. C. Kirkup and M. A. Riley, Nature **482**, 412 (2004).

[76] G. Szabo, A. Szolnoki, and R. Izsák, J. Phys. A **37**, 2599 (2004).

[77] A. Szolnoki and G. Szabó, Phys. Rev. E **70**, 027101 (2004).

[78] T. Reichenbach, M. Mobilia, and E. Frey, Phys. Rev. E **74**, 051907 (2006).

[79] J. C. Claussen and A. Traulsen, Phys. Rev. Lett. **100**, 058104 (2008).

[80] D. Semmann, H.-J. Krambeck, and M. Milinski, Nature **425**, 390 (2003).

[81] B. Bollobás, *Random Graphs*, (Cambridge University Press, Cambridge, 2001).

[82] M. E. J. Newman, Phys. Rev. Lett. **89**, 258701 (2003).

[83] J. J. Ramasco, S. N. Dorogovtsev, and R. Pastor-Satorras, Phys. Rev. E **70**, 036106 (2004).

[84] P. M. Gleiser, J. Stat. Mech. Theor. Exper. P09020 (2008).

[85] S. N. Dorogovtsev, Phys. Rev. E **69**, 027104 (2004).

[86] M. E. J. Newman, Phys. Rev. E **64**, 025102(R) (2001).

[87] http://www.imdb.com/

[88] http::://www.arxiv.org/

[89] T. Zhou, J. Ren, M. Medo, and Y.-C. Zhang, Phys. Rev. E **76**, 046115 (2007).

[90] A. Capocci, V. D. P. Servedio, F. Colaiori, L. S. Buriol, D. Donato, S. Leonardi, and G. Caldarelli, Phys. Rev. E **74**, 036116 (2006).

[91] R. Guimerá, B. Uzzi, J. Spiro, and L. A. N. Amaral, Science **308**, (607).

[92] M. Tomassini, L. Luthi, M. Giacobini, and W. B. Langdon, Genet. Prog. Evol. Mach. **8**, 97 (2007).

[93] F. Peruani, M. Choudhury, A. Mukherjee, and N. Ganguly, Europhys. Lett. **79**, 28001 (2007).

[94] M. Choudhury, N. Ganguly, A. Maiti, A. Mukherjee, L. Brusch, A. Deutsch, and F. Peruani, e-print, arXiv/0811.0499.

[95] A. K. Chandra, K. B. Hajra, P. K. Das, and P. Sen, Int. J. Mod. Phys. C **18**, 1157 (2007).

[96] G. Palla, I. Derényi, I. Farkas, and T. Vicsek, Nature **435**, 814 (2005).

[97] J. J. Ramasco and S. A. Morris, Phys. Rev. E **69**, 016122 (2006).

[98] L. C. Freeman, Sociometry **40**, 35 (1977).

[99] R. Anderson and R. M. May, *Infectious Diseases of Human, Dynamics and Control*, (Oxford University Pres, Oxford, 1995).

[100] I. Hanski, J. Alho, and A. Moilanen, Ecology **81**, 239 (2000).

[101] D. Dhar, P. Shukla, and J. P. Sethna, J. Phys. A **45**, 5259 (1997).

[102] R. Pastor-Satorras and A. Vespignani, Phys. Rev. Lett. **86**, 3200 (2001).

[103] K. Sato, H. Matsuda, and A. Sasaki, J. Math. Biol. **32**, 251 (1994).

[104] O. Ovaskainen, K. Sato, J. Bascompte, and I. Hanski, J. Theor. Biol. **25**, 92 (2002).

[105] J. Marro and R. Dickman, *Nonequilibrium Phase Transitions in Lattice Models*, (Cambridge University Press, Cambridge, 1999).

[106] K. Sato and N. Konno, J. Phys. Soc. Japan **64**, 1866 (1995).

[107] K. Sato, N. Konno, and T. Yamaguchi, Mem. Muroran Inst. Tech. **47**, 109 (1997).

[108] D. ben-Avraham and J. Köhler, Phys. Rev. A **45**, 8358 (1992).

[109] M. Boguña, R. Pastor-Satorras, and A. Vespignani, Phys. Rev. Lett. **90**, 028701 (2003).

[110] C. Castellano and R. Pastor-Satorras, Phys. Rev. Lett. **96**, 038701 (2006).

[111] M. Ha, H. Hong, and H. Park, Phys. Rev. Lett. **98**, 028801 (2007).

[112] C. Castellano and R. Pastor-Satorras, Phys. Rev. Lett. **98**, 028802 (2007).

[113] C. Castellano and R. Pastor-Satorras, Phys. Rev. Lett. **100**, 148701 (2008).

[114] A. Traulsen and J. C. Claussen, Phys. Rev. E **70**, 046128 (2004).

[115] J. E. Satulovsky and T. Tomé, Phys. Rev. E **49**, 5073 (1994).

[116] T. Tomé and K. C. de Carvalho, J. Phys. A Math. Gen. **40**, 12901 (2007).

[117] E. Arashiro, A. L. Rodrigues, M. J. de Oliveira, and T. Tomé, Phys. Rev. E **77**, 061909 (2008).

[118] M. Pascual, P. Mazzega, and S. A. Levin, Ecology **82**, 2357 (2001).

[119] O. Ovaskainen and S. Cornell, Proc. Natl. Acad. Sci. U.S.A. **103**, 12781 (2006).

[120] J. A. Acebrón, L. L. Bonilla, C. J. P. Vicente, F. Ritort, and R. Spigler, Rev. Mod. Phys. **77**, 137 (2005).

[121] I. Hanski, M. Kuussaari, and M. Nieminen, Ecology **75**, 747 (1994).

[122] D. T. Gillespie, J. Comput. Phys. **22**, 403 (1976).

[123] D. T. Gillespie, J. Phys. Chem. **81**, 2340 (1977).

[124] T. Reichenbach, M. Mobilia, and E. Frey, Phys. Rev. Lett **99**, 238105 (2007).

[125] W. G. Dantas, M. J. de Oliveira, and J. F. Stilck, J. Stat. Mech. Theor. Exper. P08009 (2007).

[126] A. Messer and H. Hinrichsen, J. Stat. Mech. Theor. Exper. P04024 (2008).

[127] M. Berr, T. Reichenbach, M. Schottenloher, and E. Frey, Phys. Rev. Lett. **102**, 048102 (2009).

[128] T. Antal, M. Droz, A. Lipowski, and G. Ódor, Phys. Rev. E **64**, 036118 (2001).

[129] H. Reinhardt, F. Böhm, B. Drossel, and H. Hinrichsen, Eur. Phys. J B **51**, 245 (2006).

[130] G. Grinstein, D. Mukamel, R. Seidin, and C. H. Bennett, Phys. Rev. Lett. **70**, 3607 (1993).